Exp Fluids (2007) 43:101–123
DOI 10.1007/s00348-007-0329-8

RESEARCH ARTICLE

Effect of buoyancy on the wakes of circular and square cylinders: a schlieren-interferometric study

S. K. Singh · P. K. Panigrahi · K. Muralidhar

Received: 8 February 2007 / Revised: 9 May 2007 / Accepted: 9 May 2007 / Published online: 15 June 2007

Abstract Wakes behind heated cylinders, circular, and square have been experimentally investigated at low-Reynolds numbers. The electrically heated cylinder is mounted in a vertical airflow facility such that buoyancy aids the inertia of main flow. The operating parameters, i.e., Reynolds number and Richardson number are varied to examine flow behavior over a range of experimental conditions from forced to mixed convection regime. Laser schlieren-interferometry has been used for visualization and analysis of flow structures. Complete vortex shedding sequence has been recorded using a high-speed camera. The results on detailed dynamical characteristics of vortical structures, i.e., their size, shape and phase, Strouhal number, power spectra, convection velocity, phase shift, vortex inception length, and fluctuations are reported. On heating, alteration of organized (coherent) structures with respect to shape, size and their movement is readily perceived from instantaneous Schlieren images before they reduce to a steady plume. For both cylinders, Strouhal number shows a slow increase with an increase in Richardson number. At a critical value, there is complete disappearance of vortex shedding and a drop in Strouhal number to zero. The corresponding spectra evolve from being highly peaked at the vortex shedding frequency to a broadband appearance when vortex shedding is suppressed. The geometry of vortex structures transforms to a slender shape before shedding is suppressed. At this heating level, absence of multiple peaks in power spectra at cylinder centerline indicates absence of interaction between opposite shear layers. The convection velocity of vortices increases in stream wise direction to an asymptotic value and its variation is a function of Richardson number. The convection speed abruptly falls to zero at critical Richardson number. The phase difference of shed vortices between upstream and downstream location increases with an increase in Richardson number. Velocity profiles show an increase in fluid speed and beyond the critical point, buoyancy forces add enough momentum to cancel momentum deficit due to the cylinder. Overall, the combined effect of temperature gradient on the separating shear layer velocity profile in near field and vortical structures interaction in far field influences wake instability of a heated cylinder.

Electronic supplementary material The online version of this article (doi:10.1007/s00348-007-0329-8) contains supplementary material, which is available to authorized users.

S. K. Singh · P. K. Panigrahi (✉) · K. Muralidhar
Department of Mechanical Engineering,
Indian Institute of Technology Kanpur,
Kanpur 208016, India
e-mail: panig@iitk.ac.in; extern.panigrahi@dlr.de

S. K. Singh
e-mail: sukusi@iitk.ac.in

K. Muralidhar
e-mail: kmurli@iitk.ac.in

List of symbols

C_p	specific heat of the fluid, kJ/kg °C
d	representative dimension of the cylinder (diameter for circular cylinder, edge for square cylinder), m
f_o	frequency of vortex shedding, Hz
g	gravitational acceleration, m/s^2
I	gray scale intensity value of the image
k	thermal conductivity of the fluid, W/m °C
L_f	formation length, m
L	length of the cylinder, m
n	refractive index of the working medium (air)
Pr	prandtl number ($\mu C_p/k$)
Re	Reynolds number ($U_\infty d/\nu$)

Ri	Richardson number ($dg\beta\Delta T/U_\infty^2$)
St	Strouhal number ($f_o d/U_\infty$)
t	time, s
T	temperature, °C
T_w	cylinder surface temperature, °C
T_∞	free-stream temperature, °C
T_{eff}	effective temperature, $(T_\infty + 0.28(T_w - T_\infty))$ °C
T_{film}	film temperature, $(T_w + T_\infty)/2$ °C
T^*	temperature ratio $[(T_w + 273)/(T_\infty + 273)]$
ΔT	$T_w - T_\infty$, °C
ΔT_ε	temperature change per fringe shift, °C
u	stream wise velocity, m/s
v	cross-stream velocity, m/s
U_∞	uniform free-stream velocity, m/s
u_c	stream wise convection velocity, m/s
x	stream wise dimension of coordinates, m
y	transverse dimension of coordinates, m
z	span wise dimension of coordinates, m

Greek symbols

ν	kinematic viscosity of the fluid, m^2/s
β	volume coefficient of thermal expansion, $°C^{-1}$
θ	non-dimensional temperature $(T - T_\infty)/(T_w - T_\infty)$
ρ	density of the fluid, kg/m^3
λ	wavelength of the laser beam, m
Φ	phase difference

Subscripts

crit	critical
w	cylinder surface
rms	root mean square
eff	refers to conditions at effective temperature
film	refers to conditions at arithmatic mean film temperature
∞	free stream

1 Introduction

Flow behind bluff bodies has received immense attention from numerical and experimental fluid dynamicists. Examples of flow past heated circular and square cylinders are seen in heat exchangers, electronic cooling, and chemical reactors. The wake of a cylinder is unstable with increasing Reynolds numbers and instability results in formation of Karman vortex street, namely, a regular pattern of alternately shed vortices. The instability is primarily responsible for unsteady forces and heat transfer from cylindrical structure. Proper understanding of wake instability mechanism is important for flow control applications. Geometry of cylinder cross-section such as square or circular affects the wake properties. For a square cross-section, its orientation with respect to the mean flow is also an important parameter.

Most studies of bluff body wakes have focused on an isothermal fluid in which no temperature difference is maintained between the body and the ambient. However, quite a few engineering applications require the knowledge of flow behavior in wakes of heated objects. When the object is heated with respect to the incoming flow, the following possibilities arise: forced convection regime, where density changes are small; mixed convection, where density changes are significant; and free convection, where density changes entirely determine the flow field. The influence of heating also depends on orientation of the flow direction with respect to the direction of gravity. Thus aiding, opposing and cross-stream buoyancy configurations are possible. Richardson number is used to characterize the buoyancy effects at a given Reynolds number. The forced convection limit has received considerable attention in literature. Literature on wakes of heated bluff bodies that are influenced by changes in fluid density is less common and is reviewed in following paragraphs.

In an earlier work, Oosthuizen and Madan (1971) studied unsteady mixed convection flow past a cylinder over a Reynolds number range of 100–300. However, their interest was to evolve an average heat transfer coefficient, but not in behavior of near wake vortices. Merkin (1977) pointed out that heating the circular cylinder delays separation and finally, the boundary layer does not separate at all. Jain and Lohar (1979) reported an increase in shedding frequency with an increase in cylinder temperature. Badr (1984) performed a numerical investigation in mixed convection regime with Reynolds number up to 40. By adding natural convection to neutrally buoyant wake, Noto et al. (1985) experimentally observed the breakdown of unsteady vortex street for heated horizontal circular and triangular cylinders. In a detailed numerical study of shedding mechanism, Chang and Sa (1990) showed the effect of aiding/opposing buoyancy for an upward flow past a hot/cold circular cylinder at a Reynolds number of 100. According to their results, heating the cylinder impedes the roll up process with subsequent degeneration of the vortex street into steady twin vortices at a critical Richardson number of 0.15. In an experimental study Michaux-Leblond and Belorgey (1997) performed an investigation of mean flow velocities in the near wake region of a heated circular cylinder. The critical value of heat input needed for the suppression of vortex street was determined. Sharma and Eswaran (2004) have numerically studied mixed convection for a square cylinder at $Re = 100$. The disappearance of vortex shedding was reported at a critical Ri of 0.15.

Based on a reduction in Reynolds number due to an increase in dynamic viscosity with increase in temperature,

Dumouchel et al. (1998) proposed an effective temperature at which the critical Reynolds numbers for unheated and heated cylinders are equal. They calculated the effective temperature as $T_{\text{eff}} = T_\infty + C \times (T_w - T_\infty)$, with $C = 0.24 \pm 0.02$ for a temperature ratio ($T^* = T_w/T_\infty$) less than 1.5. Wang et al. (2000) using the similarity concept proposed a modified value of $C = 0.28$ in the range $1.1 \leq T^* \leq 1.8$ and found a universal relationship between Strouhal number and effective Reynolds number computed with kinematic viscosity based on the effective temperature. Although above study relates suppression of instability to viscosity, this phenomenon has also been related to density change in the near wake (Yu and Monkewitz 1990; Schumm et al. 1994). Yu and Monkewitz (1990) concluded that change in stability characteristics brought about by heating is the result of a slightly modified interaction between the two mixing layers via inertial effects and not related to viscous forces; No significant discrepancy between computations based on constant and temperature dependant dynamic viscosity was obtained. Schumm et al. (1994) showed suppression of vortex shedding up to twice the critical Reynolds number (based on cold free stream) for a circular cylinder. The authors related the instability mechanism to ratio of average density in the recirculation region to free stream density. In a later study, Lecordier et al. (2000) reported suppression of vortex shedding in airflow and related it to changes in viscosity and density with temperature. An opposite trend was found in water, suggesting a dominance of viscosity and its dependence on temperature. The shape of the velocity profile is coupled with temperature field, i.e., the changes in viscosity and density due to temperature variation relate to the velocity profile and hence the instability characteristics. In a numerical study, Shi et al. (2004) separately computed the effect of dynamic viscosity and density variations with heating. The authors concluded that both factors have an essential influence on shedding frequency and other heat transfer characteristics. In a flow visualization study, Maas et al. (2003) reported heat-induced 3D-transition of vortex street in wake of a horizontal heated circular cylinder, immersed in water. The wake became three dimensional for a Richardson number >0.3 at $Re = 117$. Vit et al. (2006) investigated vortex shedding behind heated circular cylinder in the forced convection regime. They reported a universal relationship between Strouhal number and effective Reynolds number for both air and water.

The above literature reveals that a detailed experimental study of buoyancy effect on the wake structure of a heated cylinder is limited. No experimental study on vortex shedding for flow past a heated square cylinder is available. The square cylinder is fundamentally different from that of the circular cylinder due to its fixed separation point. Therefore, it is essential to compare the effect of heating on vortex shedding mechanism of the circular cylinder with that of the square. When probes such as hot-wire is used, there are inherent difficulties in conducting experiments with a strongly heated cylinder. In this context, optical techniques are non-intrusive and are better suited. The laser schlieren technique has been used in the present study for characterization of the heated wake of circular and square cylinders. The schlieren technique along with a high-speed camera enables visualization of spatial and temporal structures of the flow field. The instantaneous thermal field, RMS fluctuations, power spectra, convection velocity, phase shift, and time traces have been presented for understanding the interaction of vortical structures in the near wake of heated cylinders. Details of flow mechanism that leads to the suppression of instability in heated wakes are reported. One salient feature of the present study is visual presentation of evolution in vortex structures during the vortex shedding suppression of a heated cylinder. The main motivation of our investigation is to provide new experimental information on processes and mechanisms involved in heat-induced changes of vortex structures under the influence of buoyancy.

2 Experimental details

The flow direction and the coordinate system with respect to the cylinder are shown in Fig. 1a, b. The schematic diagram of the experimental set-up and the optical measurement system used in the present study are shown in Fig. 1c. Details of the heating arrangement are shown Fig. 1d. The set-up comprises a vertical flow facility, a horizontal heated cylinder, a laser schlieren apparatus and imaging system. Experimental details with instrumentation used are discussed in the following sections.

2.1 Flow facility and heated cylinder

Experiments were performed in a vertical test cell that resembles an open circuit wind tunnel. The test cell is made of Plexiglas and consists of a settling chamber, honeycomb structure, anti-turbulence wire screens, contraction cone, test region, and outflow section. The contraction cone is connected to the settling chamber and the test section with an area contraction ratio of 4:1. A 2.25 kW centrifugal blower with its motor speed regulated by frequency-based drive (VICTOR G1000, Kirloskar Electric, Mysore, Karnataka, India) was used to maintain steady flow in the vertically upward direction. Experiments were performed in the low-velocity range of 0.13–0.27 m/s in 0.95 m long test section of 0.4×0.4 m^2 cross-section. The free stream turbulence was <0.3% and flow uniformity was better than 1% over 95% of the width (outside the wall boundary layers) for the

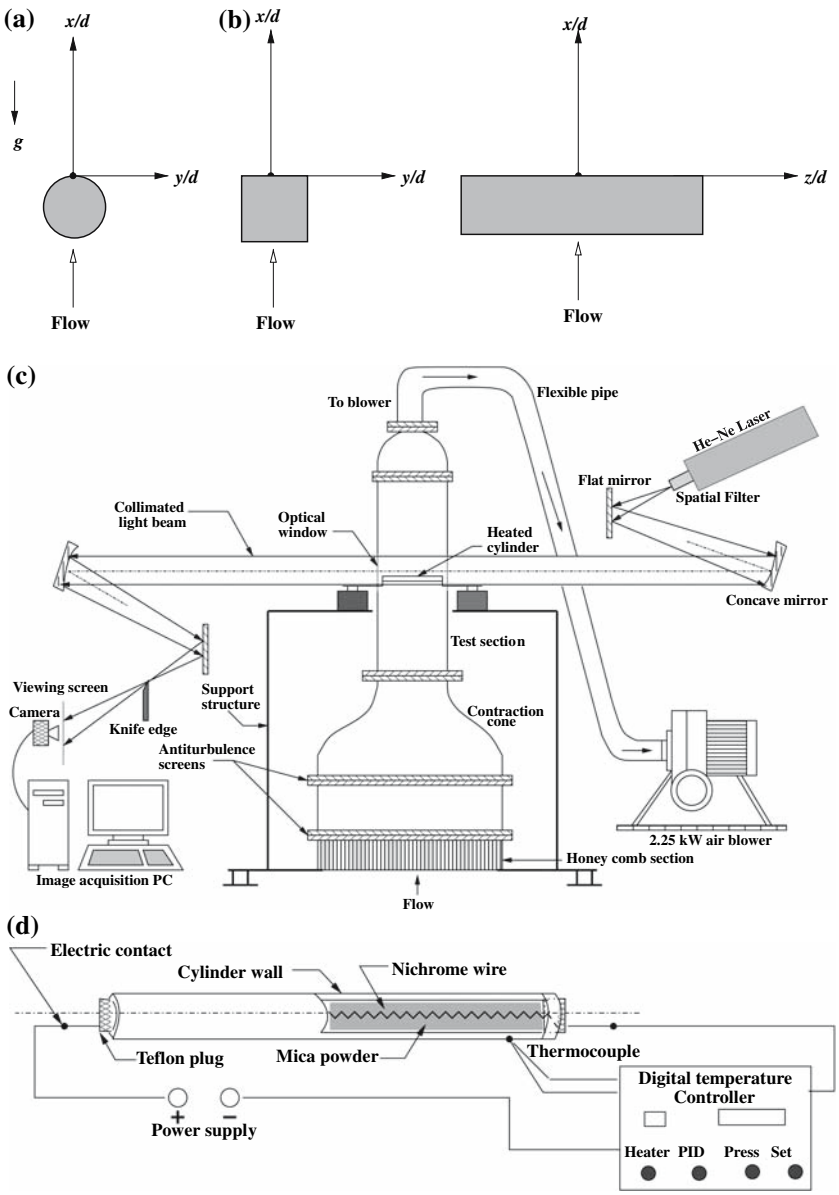

Fig. 1 Flow geometry around a heated horizontal **a** circular cylinder and **b** square cylinder; **c** Schematic diagram of the experimental setup with Z-type laser schlieren apparatus; **d** Details of the cylinder heating arrangement

velocity range considered. The free stream velocity and velocity distribution across the wake are measured by a pitot static tube connected to a high resolution digital micromanometer (FC012, Furness Controls, Tamworth, Shaffordshire, UK: 1.999 pascals) with a resolution of 0.001 Pascal. A one wire hot-wire probe (5 μm diameter, platinum-plated tungsten wire) in conjunction with a constant temperature anemometer (CTA, Model 1050, TSI, Bangalore, Karnataka, India) was used to measure turbulence intensity and power spectra. The hot-wire signal integrated over a time interval of 20 s at 1 kS/s was acquired via a PC through a 12-bit A/D card (PCI-MIO-16E-4, National instruments, Austin, TX, USA). LabVIEW was used for data collection and control. A spectrum analyzer was also used for real time spectral analysis of hot-wire signal to compute the power spectrum and hence the vortex shedding frequency.

Test cylinders, one circular (6.2 mm diameter and 390 mm long) and the other square (6.7 mm edge and 390 mm long) were employed as model bluff objects. Each cylinder was placed horizontally with its major axis and one of the faces of square cylinder at right angles to the main flow direction. The cylinders spanned the full width of the test section resulting in an aspect ratio of 65 (circular) and 60 (square) with a corresponding blockage ratio of 1.55 and 1.68%, respectively. The cylinders made of copper were well polished to remove oil and dust build-up. The square cylinder was carefully machined to produce a square section with sharp edges. Both cylinders were internally heated with a nichrome wire positioned at the axis of the cylinder tube and through out the length of the cylinder (Fig. 1d). The wire was insulated from the copper body by packing mica powder in the gap. The power to the heater was sup-

plied by a regulated DC power supply (Elnova, New Delhi, India). To reduce end heat losses, two small Teflon plugs of 5 mm length were attached to the ends of the cylinder. Two sharp metallic holders supported the cylinder at each plug through small openings in the tunnel. The surface temperature was measured using a pre-calibrated, 36-gage (AWG, 0.127 mm) chromel-alumel (type K) thermocouple flush with the cylinder using a heat-conducting epoxy. Using a DC power supply and temperature controller in a closed-loop with solid state relay circuit, the temperature of the cylinder was maintained constant with an accuracy of ±0.2°C. Temperature was measured at various axial and circumferential locations to check uniform heating of the cylinder surface. The temperature was uniform to within 0.1°C around the cylinder circumference and at all faces of the square cylinder. Temperature non-uniformities of up to ±0.3°C were recorded along the cylinder axis for the highest temperature considered.

The origin of the wake coordinate system is fixed on top surface of the cylinder at the midspan as shown in Fig. 1a, b. The x-axis is directed downstream (the stream wise direction) along the vertical. The y-axis is perpendicular (the transverse direction) to the flow and the cylinder axis. The z-axis lies on top surface of the cylinder parallel to its own axis (the span wise direction).

2.2 Optical set-up and imaging system

The flow field has been visualized using a monochrome schlieren technique. Light deflection in a variable refractive index field generated by temperature variation is captured in the schlieren image. The intensity distribution yields an integrated property of the flow field over the length of the cylinder.

The optics used in the present study consists of a Z-type 2-mirror schlieren system as shown in Fig. 1c. The optical setup comprises a continuous wave He–Ne laser light source (35 mW, 632.8 nm, Spectra-physics, Mountain View, California, CA, USA), a pair of flat and concave mirrors, a knife-edge and a viewing screen. The original laser beam is diverged by a spatial filter and falls on a flat mirror that directs it on to a concave mirror. Two f/8,160-cm focal length concave mirrors are used to collimate the light beam through the test section and then refocus it onto a knife-edge. The knife-edge is a razor blade, placed at the focal length of the second concave mirror. In the test region, flow past the heated cylinder results in a heated wake and hence density gradients prevail. The density field results in a refractive index field and hence a light intensity distribution at the image plane is obtained. As the gradients are predominantly in the vertical direction, the knife-edge is kept horizontal. The knife-edge cuts off a part of the incident light for observing the schlieren effect in the form of an intensity contrast. The initial percent cut-off is adjusted in such a way that the thermal field is imaged with good contrast but without saturating the camera.

For imaging of flow field two optical windows (BK-7, 60 mm diameter, 5 mm thickness, $\lambda/4$ flatness, Standa, Vilnius, Lithuania) have been used to facilitate passage of the laser beam through the test section. They are mounted on accurately cut seats in Plexiglas frames with Teflon tape sealing the circumference. The Plexiglas frames fit in the 10×8 cm^2 size rectangular slots, cut on opposite sides of the test section. Considerable care has been taken to ensure parallelism between two optical windows placed at the entrance and the exit of the laser beam.

A high speed CMOS sensor based monochrome camera (MC1302, Mikrotron, Unterschleissheim, Germany) with 8-bit dynamic resolution has been used to capture the sequence of schlieren images. A high knife-edge cut-off increases the sensitivity of schlieren apparatus in the sense that small density gradients in the flow can be detected. However, this setting diminishes the amount of light reaching to the camera. Short exposure time in high-speed imaging requires high light intensity to cover the full dynamic range. Hence, to balance exposure time for light intensity with high-speed imaging, an optimum is arrived at between knife-edge cut-off and frame speed to cover the full dynamic range of the camera. After various trials, the flow field was recorded at a speed of 250 frames per second and a spatial resolution of 512×512 pixels. This frame speed is well above the Nyquist criterion to capture the vortex-shedding frequency and resolve the events occurring in the development of flow structures. The camera is connected to a PC-based image acquisition system through a 64-bit frame grabber card (X64-CL, Coreco Imaging, St. Laurent, QC, Canada) and Audio capture software.

Errors in optical instrumentation are associated with misalignment of the apparatus with respect to the light beam and imperfection in the optical components. The noise in the optical signal during any stage of the experiment can be due to internal and external disturbances such as floor vibration and external convection patterns including air currents from fans used in cooling electronic components. This is particularly true for schlieren imaging of low-velocity airflow. Experiments were conducted under quiet conditions especially during recording schlieren images. The repeatability of the data presented here was ensured from many experiments performed under practically identical test conditions.

2.3 Experimental conditions

The details of the experimental conditions for circular and square cylinders are compiled in Tables 1 and 2,

respectively. Detailed experiments were performed at different flow velocities to have three Reynolds numbers each for circular and square cylinders. Of these six cases, one experiment for circular cylinder was performed in the laminar steady flow regime at $Re = 53$. Other experiments were performed in the vortex shedding regime at Reynolds numbers near $Re = 100$. To study the effect of heating at different Reynolds numbers, a total of 57 sets of experiments were performed for different cylinder temperatures ranging from 30 to 85°C. The ambient temperature was in the range 21–23°C during experiments. The Richardson number range was large enough to cover forced, mixed and buoyant convection regimes. The highest Reynolds number studied was 118, above which it was not possible to study suppression of vortex shedding by heating in view of a high temperature requirement.

For the range of Reynolds numbers studied, three-dimensional flow can be expected in the test cell. The cylinder length is quite large with respect to the cylinder diameter (aspect ratios being 65 and 60 for circular and square cylinders, respectively). Hence, wall effects are not expected to be an important factor in determining the wake behavior. The maximum Richardson number at $Re = 118$ is 0.171, a value less than 0.3 needed for heat-induced 3D-transition (Maas et al. 2003).

2.4 Formation of Schlieren-interferograms

In the schlieren technique, the light beam closer to the cylinder is refracted due to gradients in temperature, thus generating an intensity distribution on the imaging plane. Away from the cylinder surface, temperature gradients are small and the object beam passes with a small deflection through the test medium. Hence, if sufficiently long phase objects are available, the light beam away from the cylinder can act as a reference beam with which the test beam closer to the cylinder can interfere. Interference of the two portions of the light beam results in interferometric fringes. Fringes are the lines of constant optical path length. As discussed by Goldstein (1996), if the index of refraction varies only in a plane perpendicular to the beam, fringes are also contours of constant index of refraction. In ideal gas at constant pressure and constant gas composition the fringes are lines of constant temperature averaged in the viewing direction within the test cell. Thus, schlieren-interferograms provide additional information in the form of isotherms in the wake.

Schlieren interferograms are prone to errors due to the inhomogeneous distribution of background light intensity in the image plane and the reference beam non-uniformity. Therefore, all fringes are not clearly visible in the image. Brackenridge and Peterka (1967) reported that knife-edge positioned at maximum contrast could not produce a correct total fringe count. Anderson and Milton (1989) reported that Z-type concave mirror schlieren system results in astigmatic image of the source. The authors found a slight degradation of fringe visibility. As one of the reason of uneven schlieren background illuminance, Settles (2001) showed that concave mirrors used on-axis in an off-axis mirror type schlieren system lead to errors in faithful

Table 1 Experimental conditions for a circular cylinder

Test case	Cylinder diameter (mm)	Flow velocity (m/s)	Reynolds number (*Re*)	Ambient temperature °C	Test case	Cylinder diameter (mm)	Flow velocity (m/s)	Reynolds number (*Re*)	Ambient temperature °C
1	6.2	0.13	53	23	3	6.2	0.27	110	21
2	6.2	0.23	94	21					

Set number	Cylinder surface temperature °C	Richardson number (*Ri*) Case 1 (*Re* = 53)	Richardson number (*Ri*) case 2 (*Re* = 94)	Richardson number (*Ri*) case 3 (*Re* = 110)	Set number	Cylinder surface temperature °C	Richardson number (*Ri*) case 3 (*Re* = 110)
1	30	0.084	0.035	0.025	10	55	0.091
2	35	0.143	0.053	0.039	11	60	0.104
3	40	0.201	0.072	0.052	12	65	0.116
4	43	0.235			13	70	0.128
5	45		0.090		14	75	0.140
6	46	0.269			15	77	0.145
7	50	0.314	0.108	0.078	16	79	0.150
8	52		0.115		17	81	0.154
9	54		0.122		18	82	0.157

Table 2 Experimental conditions for a square cylinder

Test case	Cylinder edge (mm)	Flow velocity (m/s)	Reynolds number (Re)	Ambient temperature °C	Test case	Cylinder edge (mm)	Flow velocity (m/s)	Reynolds number (*Re*)	Ambient temperature °C
1	6.7	0.20	87	23	3	6.7	0.27	118	23
2	6.7	0.25	109	23					

Set number	Cylinder surface temperature °C	Richardson number (*Ri*) case 1 (*Re* = 87)	Richardson number (*Ri*) case 2 (*Re* = 109)	Richardson number (*Ri*) case 3 (*Re* = 118)	Set number	Cylinder surface temperature °C	Richardson number (*Ri*) case 2 (*Re* = 109)	Richardson number (*Ri*) case 3 (*Re* = 118)
1	32	0.049			13	58	0.117	
2	35	0.065	0.042	0.036	14	59		0.103
3	40	0.092	0.059		15	60	0.124	
4	41	0.097			16	63	0.133	
5	43	0.107		0.059	17	65	0.139	0.119
6	44	0.113			18	67	0.146	
7	45		0.075		19	70	0.155	
8	47	0.128			20	71		0.135
9	48	0.133			21	73	0.164	
10	50	0.143	0.092		22	76	0.173	0.148
11	51			0.081	23	82		0.163
12	55		0.108		24	85		0.171

production of light source image at the cutoff plane. The problem of fringe visibility can be more serious for imaging of a time dependent flow field, where both the object beam and to an extent the reference beam fluctuate with time. It was found in the present study that all fringes could be recovered by working with mean-removed intensity distribution in the schlieren images. The averaging had effect of eliminating time-dependent oscillations in the background intensity. The effect of processing procedure on the evaluation of schlieren interferogram of the wake of a square cylinder heated to 40°C in an ambient at 23°C is shown in Fig. 2. The Reynolds number in this experiment is 109. Figure 2a, b show the instantaneous and time-averaged schlieren images, respectively. The time-averaged schlieren interferograms have been generated from 1,250 instantaneous schlieren images, which represent 27 vortex shedding cycles. Figure 2c shows the mean removed phase averaged (over 27 vortex-shedding cycles) schlieren interferogram at the time instant corresponding to Fig. 2a. The number of fringes in Fig. 2c is higher than that in Fig. 2a indicating reduction of background noise due to phase averaging. Figure 2d shows the mean removed time averaged schlieren interferograms. The subtraction of averaged intensity from the schlieren images also improve the contrast leading to clear interferograms in Fig. 2d. We evaluate the accuracy of schlieren interferogram by comparing the actual temperature difference between the cylinder surface and the free stream with the predicted temperature difference from the number of fringes. The temperature difference per fringe shift has been calculated using the formula that includes refraction effects (Muralidhar 2001)

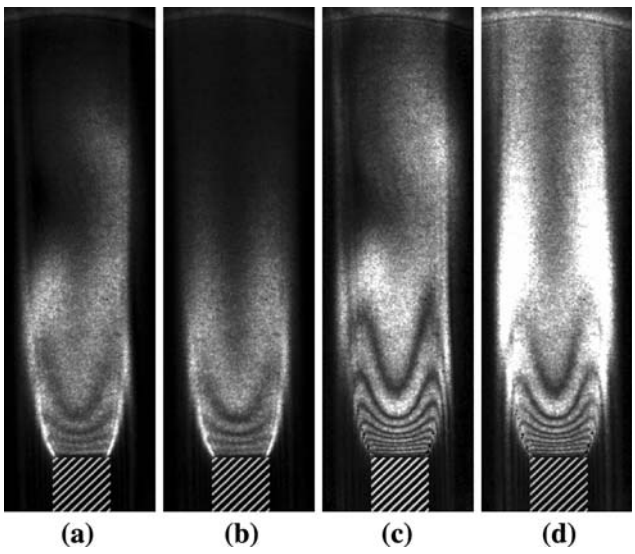

Fig. 2 **a** Instantaneous, **b** time averaged, **c** mean removed phase averaged, and **d** mean removed time averaged schlieren interferograms for a square cylinder at *Re* = 109 and *Ri* = 0.059

$$\Delta T_{\varepsilon}=\frac{1}{L\mathrm{d}n/\mathrm{d}T}\left(\lambda-\frac{1}{6n}\left(\frac{\mathrm{d}n}{\mathrm{d}T}\right)^{2}\left(\left(\frac{\partial T}{\partial x}\Big|_{2}\right)^{2}-\left(\frac{\partial T}{\partial x}\Big|_{1}\right)^{2}\right)L^{3}\right). \quad (1)$$

Here, λ is the wavelength of the laser beam, L the length of the test medium, and n the refractive index of the working medium, namely air. The predicted temperature difference is obtained by multiplying the number of fringes and the temperature difference per fringe shift.

Since the gradient in temperature field is not known before the calculation of the fringe temperature, the factor $\left(\frac{\partial T}{\partial x}|_{2}\right)^{2}-\left(\frac{\partial T}{\partial x}|_{1}\right)^{2}$ must be calculated from a guessed temperature field. The formula neglecting refraction effects for temperature difference per fringe shift $\Delta T_{\varepsilon}=\frac{\lambda/L}{\mathrm{d}n/\mathrm{d}T}$ can be used as an initial guess. The final calculation of ΔT_{ε} relies on a series of iterative steps with improved estimates of the temperature gradients. The refraction contribution in the present set of experiments was found to be quite small. A typical value of ΔT_{ε} was calculated to be 1.8°C.

Results obtained with various cylinder temperatures and Reynolds numbers are compared in Tables 3 and 4 for circular and square cylinders, respectively. There is a good match of the measured temperature difference between the cylinder surface and the free stream with that from the schlieren interferograms. A maximum difference of 8% between the actual temperature difference and that from the interferograms is to be seen in Table 3. This small difference is within the experimental uncertainty arising from errors in the measurement of cylinder surface temperature, effectiveness of the temperature controller, optical misalignment, and digitization error. Measurement of the centerline wake temperature using a thermocouple was also seen to compare well with the schlieren interferogram data. Overall, Tables 3 and 4 confirm the usefulness of the schlieren-interferometry technique.

3 Validation

An important parameter in unsteady periodic flow is the vortex shedding frequency expressed in non-dimensional form as the Strouhal number. Traditionally, hot-wire anemometry is used for obtaining the vortex shedding frequency of bluff bodies. However, the use of hot-wire anemometry is prone to large error for heated cylinder. Therefore, we have obtained the vortex shedding frequency from the intensity fluctuation of schlieren images.

The schlieren measurements have been validated from a comparison of the Strouhal number versus Reynolds number plot against data of the published literature. Strouhal number of a heated cylinder has been evaluated from a time sequence of schlieren measurements. A Fourier transform of the time series of light intensity in the schlieren images is used for spectral calculations to determine shedding frequency and hence the Strouhal number. The light intensity is averaged in a zone of 4×4 pixel to minimize the pixel-level noise. The location of the zone has been chosen to obtain clear vortex shedding frequency and is located at $2d$ in the stream wise and $0.75d$ in the transverse direction. The square cylinder is mildly heated to a temperature of 30°C in an ambient at 23°C for obtaining forced convection conditions. Considerable attention has been paid toward realizing the uniform temperature boundary condition along the cylinder span for the duration of the experiment. This is an important requirement because the schlieren image is an average obtained along the length of the cylinder. The flow velocity is varied between 0.24 and 0.54 m/s with corresponding Richardson number in the range of 0.005–0.026. Buoyancy effects can thus be neglected for the validation study. For no cylinder heating hotwire measurements have also been carried out for validation. The hotwire probe was placed at the mid-span ($z = 0$) and at a distance of $2d$ downstream from the top face of the square cylinder, offset by $0.75d$ to one side of the wake center plane.

Table 3 Circular cylinder: comparison of actual temperature difference between the cylinder surface and free stream with the measured temperature difference from evaluation of schlieren interferograms

Set number	Cylinder temperature T_w, °C	Ambient temperature T_∞, °C	Measured ΔT ($T_w - T_\infty$) °C	Number of fringes	Temperature change per fringe shift ΔT_ε, °C	ΔT from schlieren interferograms °C
1. Re = 53	30	23	7	4	1.8	7.2
	35	23	12	7	1.8	12.6
	40	23	17	10	1.8	18.0
	43	23	20	12	1.8	21.6
2. Re = 110	30	21	9	5	1.8	9
	35	21	14	8	1.8	14.4
	40	21	19	11	1.8	19.8

Table 4 Square cylinder: comparison of actual temperature difference between the cylinder surface and free stream with the measured temperature difference from evaluation of schlieren interferograms

Set number	Cylinder temperature T_w, °C	Ambient temperature T_∞, °C	Measured ΔT $(T_w - T_\infty)$ °C	Number of fringes	Temperature change per fringe shift ΔT_c, °C	ΔT from schlieren interferograms °C
1. Re = 87	40	23	17	9	1.8	16.2
	44	23	21	11	1.8	19.8
	48	23	25	14	1.8	25.2
	50	23	27	15	1.8	27
2. Re = 109	40	23	17	9	1.8	16.2
	45	23	22	12	1.8	21.6
	50	23	27	15	1.8	27

Figure 3a compares the variation of Strouhal number with Reynolds number for the square cylinder. The range of Re investigated was from 105 to 236. At low Re, the Strouhal number increases continuously with Re, and at Re = 157, the St reaches its local maximum. Beyond this Reynolds number, there is sudden reduction in its value. The magnitude and nature of variation of Strouhal number with respect to Reynolds number from hotwire measurements is in close agreement with the schlieren data. The results from the present experiments are also in excellent agreement with the experimental data of Luo et al. (2003) and numerical results of Sohankar et al. (1999). An exception is seen in the form of deviation from the results of Robichaux et al. (1999) in which low-Re data appear to be higher and higher Re data appear to be lower. The deviation is more significant for Reynolds number >200 and the largest deviation being nearly 7%. Possible explanation for this discrepancy could be differences in the aspect ratio of the model, blockage and upstream conditions. Figure 3a, however, broadly confirms the capability of the time-sequence of schlieren images to determine Strouhal number and has been used for calculation of Strouhal number for other set of experiments. This approach has been further adapted to record statistics of flow fluctuations in the cylinder wake.

4 Results and discussion

Physical picture of vertical flow around a heated cylinder can be visualized as follows. Fluid particles accelerate in the boundary-layers around the cylinder. Increase in kinetic energy delays the point of separation, thus raising average base pressure. Consequently, vortices formed in the wake are weakened by heating, ultimately resulting in complete suppression of vortex shedding. At elevated cylinder temperatures, vortices are weak and thus result in diminishing cross-stream transport. It is a minimum when vortex shedding is absent. The progression toward state of no vortex shedding is, however, not monotonic. At mild heating levels, acceleration of fluid particles in the shear layers enhances vortex strength and moderately increases cross-stream diffusion. These trends are discussed in detail in the following sections.

Experiments have been conducted over a wide range of Reynolds numbers (53–118) and Richardson numbers (0.025–0.314) for cylinders of both circular and square cross-sections. Results obtained from these experiments have been jointly presented in the following sequence: (a) Suppression of vortex shedding, (b) Instantaneous visualization images, (c) Time-averaged schlieren images, (d) Vortex formation length, (e) Distribution of light intensity fluctuations, (f) Power spectra and time traces, (g) Velocity profiles, (h) Temperature distribution, (i) Convection velocity and phase shift, and (j) Instability mechanism.

4.1 Suppression of vortex shedding

Suppression of vortex shedding behind a heated cylinder has been demonstrated by schlieren image visualization, time traces of light intensity, corresponding power spectra, and Strouhal number. The lowest flow velocity achieved in the flow is 0.13 m/s, corresponding to a Reynolds number of 53 for the circular cylinder. At this Reynolds number, no vortex shedding was seen for Richardson number ranging from 0.084 to 0.314. Hence the Strouhal number is zero. Regular vortex shedding and a definite Strouhal number was noted at other Reynolds numbers namely, Re = 94 and 110 for the circular cylinder and Re = 87, 109, and 118 for the square cylinder. At these Reynolds numbers, vortex shedding was suppressed at an elevated Richardson number, the corresponding Strouhal number becoming zero.

The Strouhal number variation with respect to Richardson number for fixed Reynolds numbers is presented in Fig. 3b, c, respectively, for circular and square cylinders. Both figures show a small initial increase in Strouhal number with Richardson number at each Reynolds number. The Strouhal number is higher at higher Reynolds

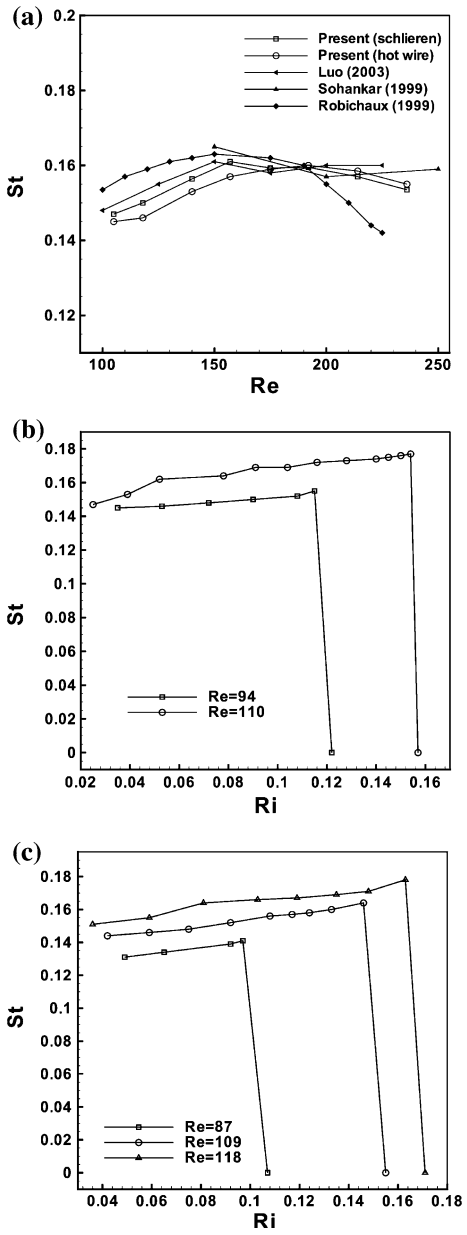

Fig. 3 **a** Variation of Strouhal number with Reynolds number for a square cylinder and comparison with literature; **b** Strouhal number variation with Richardson number for a circular cylinder; **c** Strouhal number variation with Richardson number for a square cylinder

numbers. In this Reynolds number range, the Strouhal number follows an identical trend with respect to Reynolds number for the heated cylinder as for an unheated cylinder, Fig. 3a (Luo et al. 2003; Sohankar et al. 1999; Robichaux et al. 1999). Hence, it is seen that the effect of Reynolds number on Strouhal number is not affected by heating till the critical point is reached. The increase in Strouhal number with increase in heating level, i.e., increase in Richardson number takes place for both circular and square cylinder (Fig. 3b, c) till a critical value of Richardson number is reached. After the critical Richardson number, vortex shedding stops abruptly and Strouhal number falls to zero. The critical Richardson number at which suppression of vortex shedding takes place depends on Reynolds number. It is higher at higher Reynolds numbers. This is an indication that critical Richardson number is not a universal property for the suppression of vortex shedding and is Reynolds number dependent. Earlier numerical study by Chang and Sa (1990) has also shown increase in Strouhal number with increase in Richardson number for circular cylinder. The present experimental study confirms this trend for both circular and square cylinders.

Table 5 presents critical Richardson number as a function of Reynolds number for both circular and square cylinders. The disappearance of vortex shedding takes place at $Ri = 0.122$ for $Re = 94$ and at $Ri = 0.157$ for $Re = 110$ for circular cylinder. The critical Ri-values for a square cylinder are equal to 0.107, 0.121, 0.140, 0.155, and 0.171 for $Re = 87$, 94, 103, 109, and 118, respectively. The critical Richardson numbers for a square cylinder are quite close to those of a circular cylinder at comparable Reynolds numbers. This indicates that both circular and square cylinders share similar flow phenomena for vortex shedding suppression. From numerical simulation, Merkin (1977) reported delay in separation location over circular cylinder due to heating. For a square cylinder, separation location is fixed at the edge of the cylinder. Identical critical Richardson number for both circular and square cylinder indicates that shift in separation location is not an important criterion responsible for suppression of vortex shedding. Noto et al. (1985) from the comparison of circular and triangular cylinder also attributed the vortex breakdown to acceleration of velocity and not the shift in separation point.

4.1.1 *Effective Reynolds number*

An effective Reynolds number using the kinematic viscosity calculated at effective temperature has been used in the literature (see Introduction for details) for characterization of the heated cylinder wake. Dumouchel et al. (1998) defined the effective temperature as the temperature needed to increase the kinematic viscosity of air for calculation of effective Reynolds number (Re_{eff}) at the onset of vortex shedding. Wang et al. (2000) showed a universal relationship between Strouhal number and effective Reynolds number. The above two experimental studies were carried out in the forced convection regime for a circular cylinder in a horizontal flow configuration. In the present study, the cylinder is mounted in a vertical flow configuration, i.e., buoyancy force adds to the main flow. We have investigated in both forced convection ($Ri < 0.1$) and mixed convection ($Ri > 0.1$) regimes. Therefore, we have investigated the critical Reynolds number concept

Table 5 Critical Richardson number (Ri_{crit}) and critical Reynolds number calculated using kinematic viscosity of air at T_w, T_{film}, and T_{eff} at different free stream velocities for circular and square cylinders

Set number	Cylinder geometry	U_∞ (m/s)	Re_∞	Ri_{crit}	T_∞, °C	T_w, °C	T^*	T_{film} °C	T_{eff}, °C	Re_w	Re_{film}	Re_{eff}
1.	Circular	0.23	94	0.122	21	54	1.11	37.5	30.2	78	85	89
2.	Circular	0.27	110	0.157	21	82	1.21	51.5	38.1	79	92	100
3.	Square	0.20	87	0.107	23	43	1.07	33	28.6	78	82	84
4.	Square	0.22	94	0.121	26	54	1.09	40	33.8	80	87	90
5.	Square	0.24	103	0.140	26	65	1.13	45.5	36.9	82	92	96
6.	Square	0.25	109	0.155	23	70	1.16	46.5	36.2	84	95	101
7.	Square	0.27	118	0.171	23	85	1.21	54	40.4	84	99	107

based on three characteristic temperatures when vortex shedding is suppressed; the cylinder surface temperature (T_w), mean film temperature (T_{film}), and effective temperature (T_{eff}).

Table 5 compares the critical Reynolds number based on three characteristic temperatures for both circular and square cylinders at different free stream velocities. For a circular cylinder, the range of variations, i.e., scatter in the critical Reynolds number calculated using the kinematic viscosity at temperatures T_w, T_{film}, and T_{eff}, respectively, is equal to 1, 7, and 11. Similarly, the scatter in the critical Reynolds number of a square cylinder is equal to 6, 17, and 23, respectively, for temperatures based on T_w, T_{film}, and T_{eff}. The greatest variation in critical Reynolds number for both circular and square cylinders is observed when T_{eff} is used for kinematic viscosity calculation. It may be noted that effective temperature (T_{eff}) used here has been obtained based on instability characteristic of heated circular cylinder in horizontal mean flow configuration. The buoyancy effect on the wake characteristics of a heated cylinder in horizontal and vertical configurations is not identical. Therefore, a large deviation in critical Reynolds number is observed at T_{eff} for the vertical cylinder configuration. The present study indicates that the cylinder surface temperature is the correct effective temperature for calculation of fluid properties and corresponding critical Reynolds number for vortex shedding suppression behind a heated cylinder is around 81.

The importance of cylinder surface temperature can be seen from the following discussion. The instability of the separating shear layer is influenced by the curvature of the velocity profile. Close to the cylinder surface, the inertia term is negligible ($u = v = 0$) and therefore from the boundary layer equation, the curvature ($\delta^2 u/\delta r^2$) of the velocity profile is primarily dependent on pressure gradient and viscous force. Hence, the viscous force calculated using the viscosity at cylinder surface temperature properly represents the wake instability. For the horizontal mean flow configuration, the overall wake instability is influenced by the contribution of buoyant flow from the lower shear layer to the upper shear layer. In contrast, for a vertical flow configuration, both the shear layers are primarily influenced by the upstream conditions, i.e., the cylinder surface temperature.

4.2 Instantaneous visualization images

The changes in organized wake structures with respect to shape, size and their movement is readily perceived from instantaneous schlieren images before the wake degenerates into a steady plume. Figures 4 and 5 show the instantaneous schlieren images as a function of Richardson number for the circular and square cylinders, respectively. The corresponding Reynolds numbers for these cases are 110 and 109. For a given Richardson number, the images are separated by a time interval of one eighth of the time period of vortex shedding.

Figure 4a presents instantaneous images at a temperature of 40°C ($Ri = 0.052$). The heated wake zones, i.e., the bright zones behind the cylinder extend to a downstream distance of about $x/d = 6.0$. The far field region shows a stronger time-dependence. The near field region ($x/d < 1$) close to the cylinder is nearly stationary during the complete vortex shedding cycle. Thus, the base region of the wake shows very low levels of fluctuations. The growth of the heated shear layer on both sides of the cylinder takes place asymmetrically at different phases of the vortex shedding cycle. The instability of the growing shear layers results in the shedding of two alternate rows of vortices from the opposite side of the cylinder. Figure 4b shows instantaneous images of the cylinder wake at a surface temperature of 60°C ($Ri = 0.104$). Vortex shedding at this higher Richardson number is more distinct. Clear fringes are visible within the near-wake indicating presence of temperature variation inside the vortex. Figure 4c shows the time-sequence of schlieren interferograms behind the circular cylinder at a surface temperature of 75°C ($Ri = 0.140$). Regular vortex shedding with a higher number of fringes when compared to the smaller temperature level ($Ri = 0.104$) is seen here. The vortex is not an

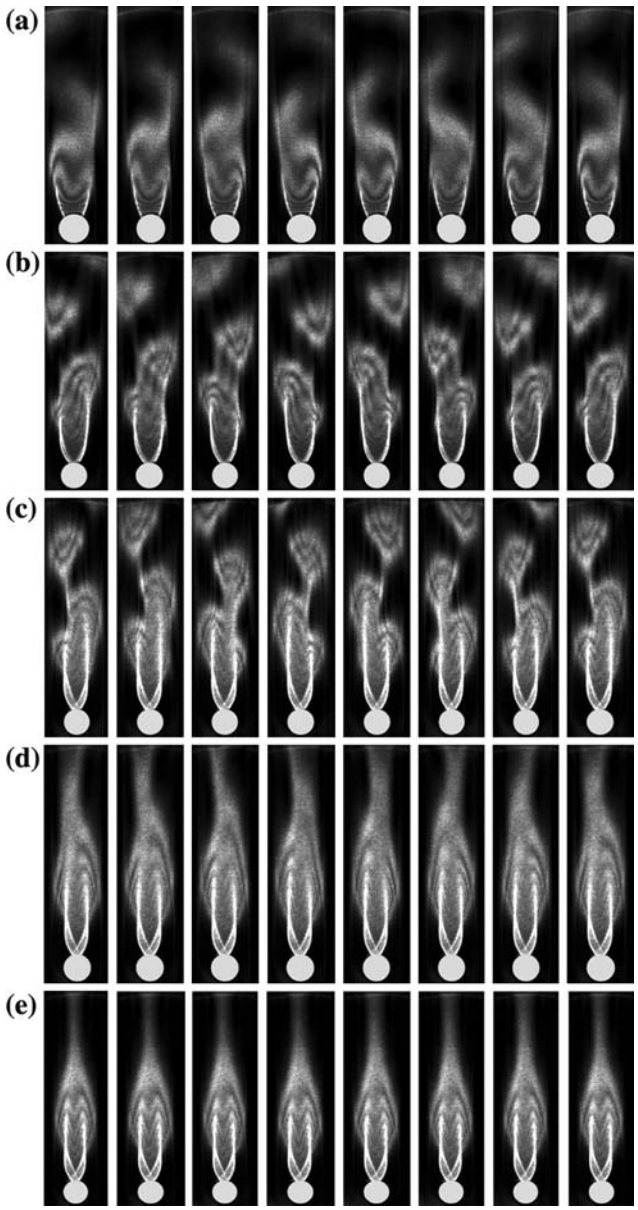

Fig. 4 Instantaneous schlieren images (**a–e**) for a circular cylinder separated by a time interval of one-eighth of the time period of vortex shedding at $Re = 110$. **a** $Ri = 0.052$, **b** $Ri = 0.104$, **c** $Ri = 0.140$, **d** $Ri = 0.150$, and **e** $Ri = 0.157$. For $Ri \geq 0.157$, images show steady state

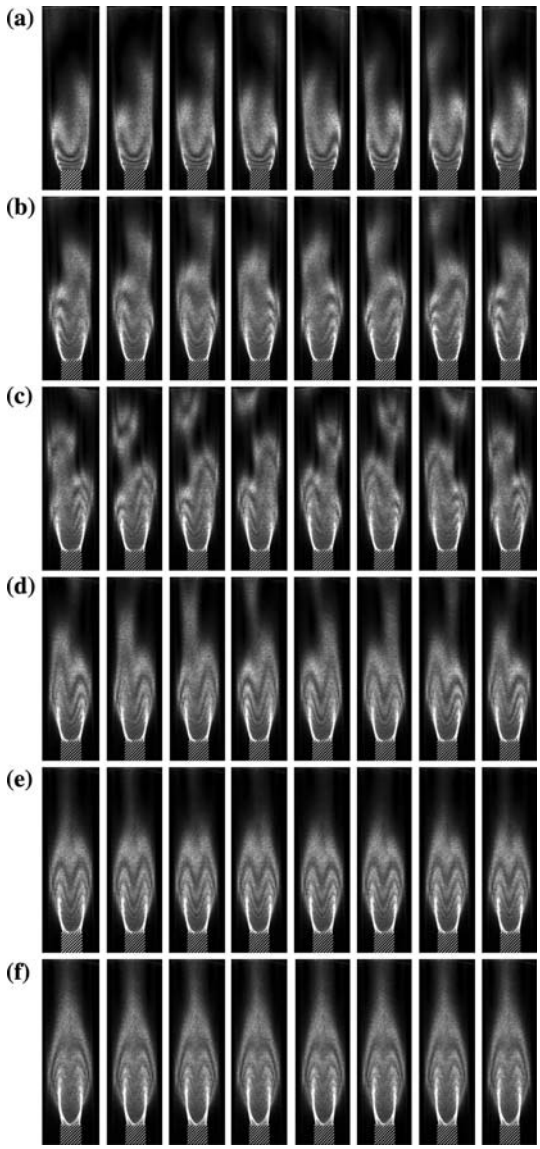

Fig. 5 Instantaneous schlieren images (**a–f**) for a square cylinder separated by a time interval of one-eighth of the time period of vortex shedding at $Re = 109$. **a** $Ri = 0.059$, **b** $Ri = 0.108$, **c** $Ri = 0.117$, **d** $Ri = 0.124$, **e** $Ri = 0.133$, and **f** $Ri = 0.155$. For $Ri \geq 0.155$, images show steady state

isothermal packet of fluid; rather it is the recirculation bubble with a temperature distribution within. The instability mechanisms that result in the detachment of the vortex continue to be quite similar at Richardson numbers up to 0.140. The visualization images during one shedding cycle for the cylinder temperature of 79°C ($Ri = 0.150$) are shown in Fig. 4d. The vortex shedding structure is altered at this Richardson number compared to the earlier cases. The alternate shedding pattern observed at lower Richardson numbers is now replaced by a thin plume, which slowly oscillates in the transverse direction. The interferograms in the near field region of the cylinder fluctuate in phase with the cross-stream oscillation of the thin plume region. The schlieren-interferograms at a higher surface temperature of 82°C ($Ri = 0.157$) are presented in Fig. 4e. The thin plume in the far field region is now steady, aligned with the cylinder mid-plane. The plume is thinner compared to that at $Ri = 0.150$. The interferograms do not oscillate any longer and the wake can be termed as steady.

Figure 5a presents the visualization images for a square cylinder when its surface temperature is equal to 40°C ($Ri = 0.059$). The oscillation in the far field region with

vortex shedding from the opposed shear layers is visible. Figure 5b shows the instantaneous schlieren images at a surface temperature of 55°C (Ri = 0.108). Compared to the lower Richardson number, the images show vortex shedding with greater clarity. The size of the detached shear layer is higher at higher Richardson number. Vortex shedding here is less distinct for the square cylinder when compared to the circular cylinder (Fig. 4b). The schlieren-interferograms at the cylinder temperature of 58°C (Ri = 0.117) for the square cylinder in Fig. 5c shows distinct and regular vortex shedding. Hence, the increase in heating level regularizes the vortex shedding process, though mixed convection influences the interaction among the shed vortices. Figure 5d shows schlieren-interferograms for a cylinder temperature of 60°C (Ri = 0.124). The shape and size of the detached shear layer at this Richardson number is distinctly different from that at the lower Richardson number (Ri = 0.117). The detached shear layer arising from the vortex shedding process is more elongated at the higher Richardson number. The instantaneous images at higher cylinder temperature of 63°C (Ri = 0.133) in Fig. 5e indicate mild unsteadiness of the shear layer. Figure 5f shows the schlieren images at cylinder temperature of 70°C (Ri = 0.155). Here, two shear layers have merged into one leading to a single steady plume at the center of the cylinder. The interferograms in the near field region are also steady in time, indicating complete steadiness of the wake. However, the plume extends farther downstream for the higher Richardson number (Ri = 0.155) when compared to the lower (Ri = 0.133).

The schlieren interferograms of both circular and square cylinder show similar vortex structures as a function of heating level, i.e., Richardson number. A small increase in cylinder surface temperature leads to regular vortex shedding initially due to the added flow by buoyancy forces. Further increase in heating level leads to the appearance of plume-like structures which diffuse the vorticity content of the separating shear layer, ultimately resulting in suppression of vortex shedding.

4.3 Time averaged schlieren-images

The time-averaged schlieren images provide information about the stream wise and transverse extent of the heated cylinder wake and can be used as an indicator of wake mixing. The time averaged schlieren images for the circular and square cylinders are presented in Figs. 6 and 7 as a function of Reynolds number and Richardson number.

For a circular cylinder, the stream wise dimension of the wake zone increases with an increase in Richardson number for all Reynolds numbers (Fig. 6). For Re = 53, the time-averaged schlieren images look identical to the instantaneous images because the wake is steady. At this Reynolds number, the length of the base region increases with Ri. The transverse extent of the wake in the far field region also increases with an increase in Richardson number but subsequently reduces. The transverse spread of the wake indicates the lateral movement of the shear layer during vortex shedding. The suppression of vortex shedding leads to a reduction in growth of the shear layer and a

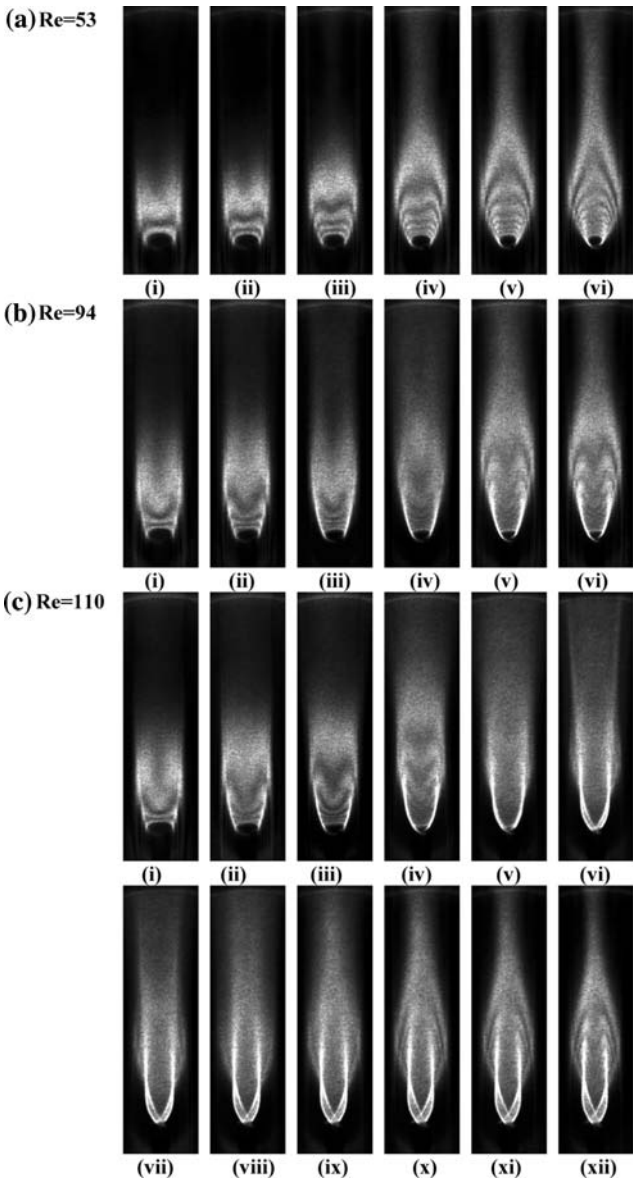

Fig. 6 Circular cylinder: time-averaged schlieren images as a function of Reynolds number and Richardson number. **a** Re = 53: (i) Ri = 0.084, (ii) Ri = 0.143, (iii) Ri = 0.201, (iv) Ri = 0.235, (v) Ri = 0.269, (vi) Ri = 0.314; **b** Re = 94: (i) Ri = 0.035, (ii) Ri = 0.053, (iii) Ri = 0.072, (iv) Ri = 0.090, (v) Ri = 0.115, (vi) Ri = 0.122; **c** Re = 110: (i) Ri = 0.025, (ii) Ri = 0.039, (iii) Ri = 0.052, (iv) Ri = 0.078, (v) Ri = 0.091, (vi) Ri = 0.116, (vii) Ri = 0.128, (viii) Ri = 0.140, (ix) Ri = 0.145, (x) Ri = 0.150, (xi) Ri = 0.154, (xii) Ri = 0.157

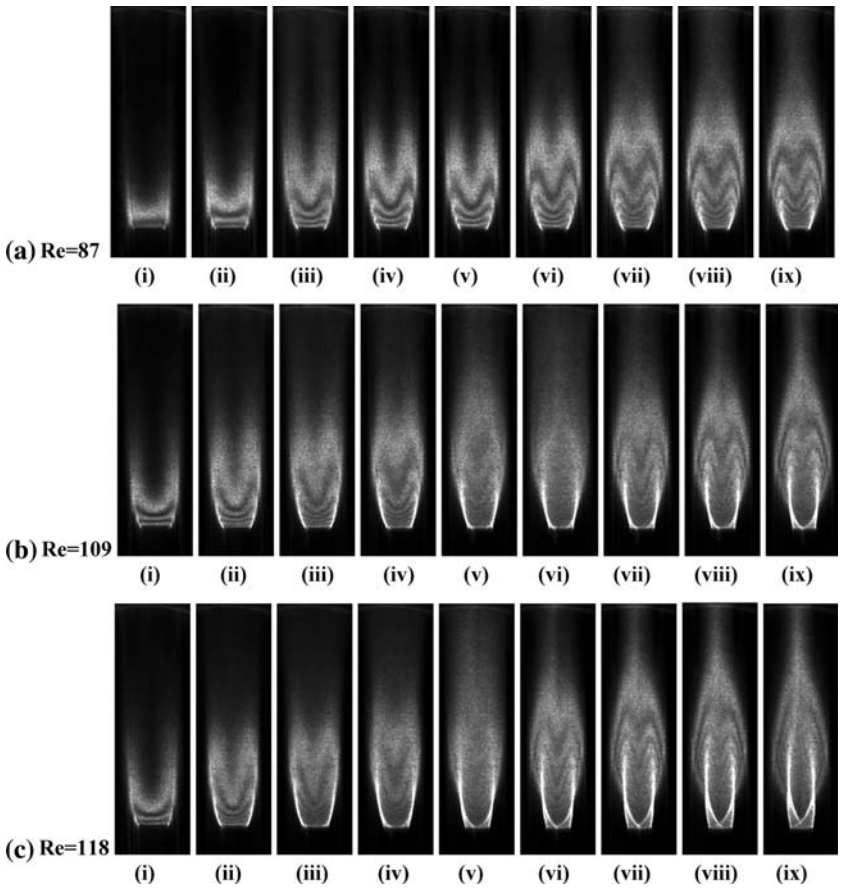

Fig. 7 Square cylinder: time-averaged schlieren images as a function of Reynolds number and Richardson number. **a** Re = 87: (i) Ri = 0.049, (ii) Ri = 0.065, (iii) Ri = 0.092, (iv) Ri = 0.097, (v) Ri = 0.107, (vi) Ri = 0.113, (vii) Ri = 0.128, (viii) Ri = 0.133, (ix) Ri = 0.143; **b** Re = 109: (i) Ri = 0.042, (ii) Ri = 0.059, (iii) Ri = 0.075, (iv) Ri = 0.092, (v) Ri = 0.108, (vi) Ri = 0.117, (vii) Ri = 0.124, (viii) Ri = 0.133, (ix) Ri = 0.155; **c** Re = 118: (i) Ri = 0.036, (ii) Ri = 0.059, (iii) Ri = 0.081, (iv) Ri = 0.103, (v) Ri = 0.119, (vi) Ri = 0.135, (vii) Ri = 0.148, (viii) Ri = 0.163, (ix) Ri = 0.171

thinner plume at the far field region in the centerline of the cylinder is obtained.

Time averaged schlieren images for the square cylinder at various Reynolds numbers are compared in Fig. 7 as a function of Richardson number. Heat transfer from the cylinder to the fluid is by the vortices within the shear layer and is a function of time. In a time-averaged sense, it leads to a high-temperature gradient in the separated shear layers as heat is carried away from the cylinder surface by the detached vortices. The presence of a dark zone between the two opposite shear layer at the lower Richardson number indicates only a small time-dependent interaction between the two. However, for higher Richardson number, the two opposed shear layers interact, merge, and form a single plume-like structure without any separation. The transverse extent of the plume in the far field region increases with an increase in Richardson number. This is due to an increase in the diffused width of the shear layers by buoyancy in the regular vortex shedding regime. Subsequent increase in cylinder temperature leads to aperiodic vortex shedding, while the final suppression leads to reduction in plume size.

The general shape and structure of the wake of the square cylinder is similar to that of the circular cylinder. The only difference is seen in the forced convection regime where buoyancy effects are not significant. Here, the individual shear layers of the square cylinder are non-interacting due to the definite points of separation. For a circular cylinder the points of separation move with an increase in Richardson number. The transitional behavior toward the mixed convection regime and finally to free convection are, however, quite similar.

4.4 Vortex formation length

The stream wise location of peak in rms velocity along the centerline of a cylinder corresponds to the point of vortex shedding and hence the vortex formation length. Konstantinidis et al. (2003) have presented the vortex formation length from the locations of peaks in the u_{rms} and v_{rms} along the cylinder centerline. It can be assumed that the intensity fluctuation in schlieren images is directly related to the temperature fluctuation and indirectly related to velocity fluctuation. We have obtained the vortex formation length based on the peak intensity fluctuation gradient of schlieren images at a small offset location, i.e., y/d = 0.25 from the cylinder centerline. The vortex formation lengths (L_f) recorded in various experiments are compared in Tables 6 and 7 for the circular and the square cylinders, respectively. The vortex formation length is a function of cylinder surface temperature and hence

Table 6 Vortex formation length as a function of Reynolds number and cylinder surface temperature for a circular cylinder

Cylinder surface temperature °C	L_f/d Re = 94	L_f/d Re = 110	Cylinder surface temperature °C	L_f/d Re = 110
30	1.0	1.0	60	1.9
35	1.5	1.8	70	2.2
40	1.5	2.2	75	2.4
45	1.8		77	2.9
50	2.7	2.9	79	3.6
52	3.0		81	3.6
54	3.0		82	3.6

Richardson number. For a low-Richardson number, i.e., at 30 and 35°C cylinder surface temperature, the vortex formation length, L_f/d = 1.0 and 0.6 for the circular and square cylinder, respectively. Konstantinidis et al. (2003) reported L_f/d to be in the range of 1–2 for a circular cylinder, which is comparable to the value obtained in our study. For both cylinders, the formation length increases with Richardson number and approaches an asymptotic value for each Reynolds number. The asymptotic formation lengths (L_f/d) are 2.7, 3.5, and 3.9 for Re = 87, 109, and 118 for the square cylinder. For circular cylinder, these values are 3.0 and 3.6 at Re = 94 and Re = 110, respectively. Similar values of the asymptotic formation length at around equal Reynolds numbers indicate the possible similarity in the vortex shedding mechanisms of the square and circular heated cylinders. This is supported by similarity in the power spectra, time traces and schlieren visualization images of heated circular and square cylinder. Vortex formation is suppressed at near-equal critical points by the action of buoyancy (Fig. 3b, c).

The critical Richardson number at which suppression of vortex shedding takes place is higher at higher Reynolds numbers. Simultaneously, the Strouhal number prior to suppression is also higher. Hence, the formation length seems to be correlated in fundamental terms to the critical Richardson number and Strouhal number. An increase in fluid speed in a highly buoyant flow field can explain longer distances traversed (for L_f) as well as a lower time period (higher Strouhal number). The increase in size of the vortex formation region with an increase in the heating level can be related to the delay in transition of the separating shear layer. Buoyancy has effect of diffusing the vorticity content inside the shear layer and the buoyant plume reduces the interaction between the opposite shear layer at both sides of the cylinder. After the suppression in vortex shedding, the RMS light intensity distribution is primarily related to the small scale vorticity production due to shear within the recirculation zone, bound on each side by the shear layers.

4.5 Distribution of light-intensity fluctuations

Since light measurements are inertia free, time-dependent fluctuations in light intensity from schlieren interferograms are essentially due to the temperature fluctuations. As the working fluid is air with a Prandtl number of the order of unity, these can be further correlated to velocity fluctuations outside the recirculation zone, where advection effects are expected to be much larger than diffusion. The influence of heating on wake fluctuations of circular and square cylinders is of interest in the present section.

The RMS (mean-removed) profiles of the fluctuating light intensity in the stream wise direction (x/d) at different transverse locations (y/d) are presented in Figs. 8 and 9 for the circular and square cylinders, respectively. For both cylinders, the intensity of fluctuations is small in the near field region ($x/d \leq 3$) very close to the cylinder surface. The instantaneous images in Figs. 4 and 5 also show steady fringes in the near field region, supporting the trends in RMS intensity of Figs. 8 and 9. The jump in the rms

Table 7 Vortex formation length as a function of Reynolds number and cylinder surface temperature for a square cylinder

Cylinder surface temperature °C	L_f/d Re = 87	L_f/d Re = 109	L_f/d Re = 118	Cylinder surface temperature °C	L_f/d Re = 109	L_f/d Re = 118
35	0.6	0.6	0.6	60	3.1	
40	1.4	1.2		63	3.2	
43	1.9		1.4	65	3.2	2.5
45		1.9		67	3.4	
47	2.4			70	3.5	
50	2.7	2.3		71		3.4
51			1.7	73	3.5	
55		2.9		76	3.5	3.7
58		2.4		82		3.8
59			2.3	85		3.9

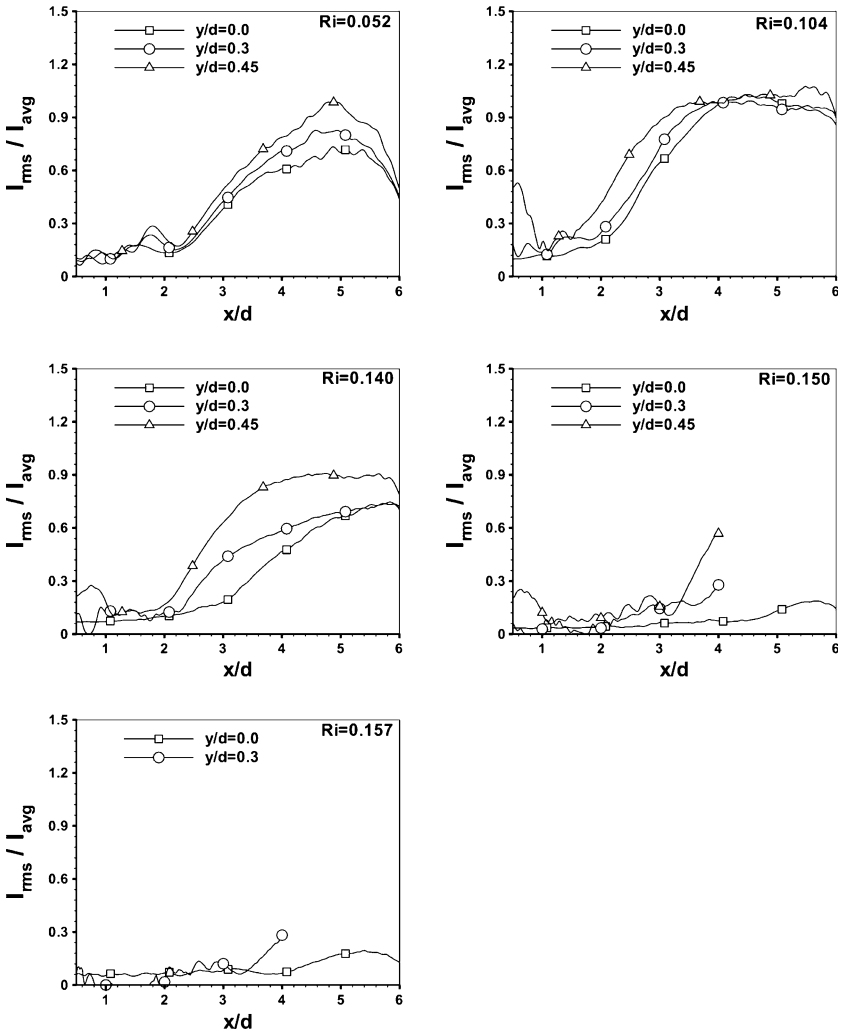

Fig. 8 Circular cylinder: evolution of the RMS intensity (I_{rms}/I_{avg}) in the stream wise direction at various transverse locations, Re = 110. Functional dependence on Richardson number is shown

intensity magnitude is due to inception of vortex shedding and the corresponding *x/d* location is termed as the vortex inception length. The RMS values are higher in the far field region where the flow is driven by vortex shedding. The unsteadiness of this region was also to be seen in the schlieren images of Figs. 4 and 5. Starting from a low value, the RMS light intensity is seen to increase asymptotically to a maximum in the stream wise direction. The RMS intensity is also the lowest along the mid-plane (y/d = 0) and increases toward the shear layer (y/d = 0.45). RMS intensities are uniformly low after vortex shedding has been suppressed at higher Richardson number.

Figures 8 and 9 show the maximum RMS intensities to be functions of Richardson number. The maximum RMS intensity is high for sub-critical Richardson numbers that are accompanied by regular vortex shedding. The peak RMS intensity is the lowest at Ri = 0.155 for square cylinder, when vortex shedding is suppressed. The RMS intensity increases in the transverse direction away from the centerline. Factors that determine the flow fluctuation levels in the wake are (a) the average size of the shed vortex, (b) interaction between opposed vortices, and (c) the average fluid speed in the shear layers. The relative difference in magnitude of the RMS intensity between different transverse locations (y/d) is an indicator of the size and shape of the detached vortices. For elongated vortices at lower Richardson number (Fig. 9, Ri = 0.059, and 0.108) the maximum rms intensity at the center locations is lower than that inside the shear layer. At Ri = 0.117, the vortex shape is symmetric and regular compared to the lower Richardson number and the rms intensity does not vary significantly in the transverse (y/d) direction. In contrast, at Ri = 0.124 the maximum rms intensity at y/d = 0.0 is significantly lower compared to y/d = 0.3 and 0.45 locations. Figure 5d shows the reversal to slender vortex structures at this heating level (Ri = 0.124). This is also an indication of reduced interaction between neighboring shear layers at higher heating level. Lower interaction between the vortices shed from the opposed shear layers reduces the wake fluctuations.

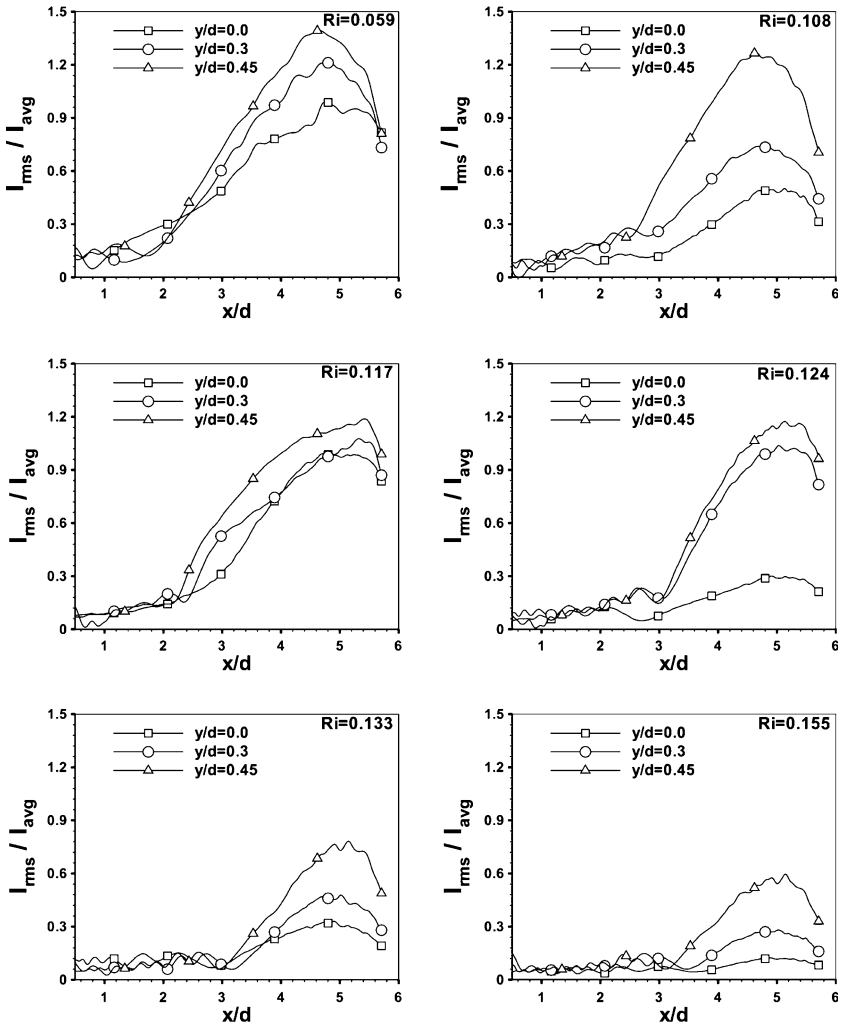

Fig. 9 Square cylinder: evolution of the RMS intensity (I_{rms}/I_{avg}) in the stream wise direction at various transverse locations, Re = 109. Functional dependence on Richardson number is shown

Figures 8 and 9 show that buoyancy influences the nature of vortex shedding and the interaction between the two shear layers leading first to a reduction of fluctuation levels and then to the suppression of vortex shedding.

4.6 Power spectra and time traces

The power spectra can show the interaction between the opposite shear layer in terms of multiple peaks. This interaction plays an important role in the inception and sustenance of vortex shedding. Therefore, the power spectra can be useful in understanding the mechanism responsible for vortex shedding suppression with an increase in Richardson number. To show the transition of bluff body wake from a clear vortex shedding mode to its suppression, the power spectra of the fluctuating light intensity in the schlieren images for square cylinders at different stream wise and transverse locations are shown in Fig. 10. The time traces corresponding to the power spectra are shown as insert in Fig. 10. The power spectra are calculated using 1,250 images acquired in 5 s. The time traces are drawn from 250 successive schlieren images for total 1 s duration. The light intensity is averaged over 4×4 pixels to diminish pixel level noise.

Figure 10a shows a dominant frequency near the shear layer at y/d = 0.75 and x/d = 2 for Ri = 0.059 indicating clear vortex shedding. The time trace of intensity shows regular variation of intensity with respect to time. The first harmonic is significant at the central region (y/d = 0) for x/d = 5.0. This may be attributed to the interaction between the vortices in the opposite shear layer. Both fundamental and harmonic modes are significant at the intermediate location (y/d = 0.35). The time traces also shows higher harmonics superimposed over the regular large-scale intensity variation. The power spectra at Ri = 0.108 in Fig. 10b shows a similar trend as that for Ri = 0.059, i.e., a dominant fundamental inside the shear layer and influence of the first harmonic in the central region. The time trace of intensity shows periodic intensity distribution at y/d = 0.35 and half-time period at y/d = 0. With further heating, Fig. 10c shows that fundamental alone is significant at all locations for Ri = 0.124. There is no significance of

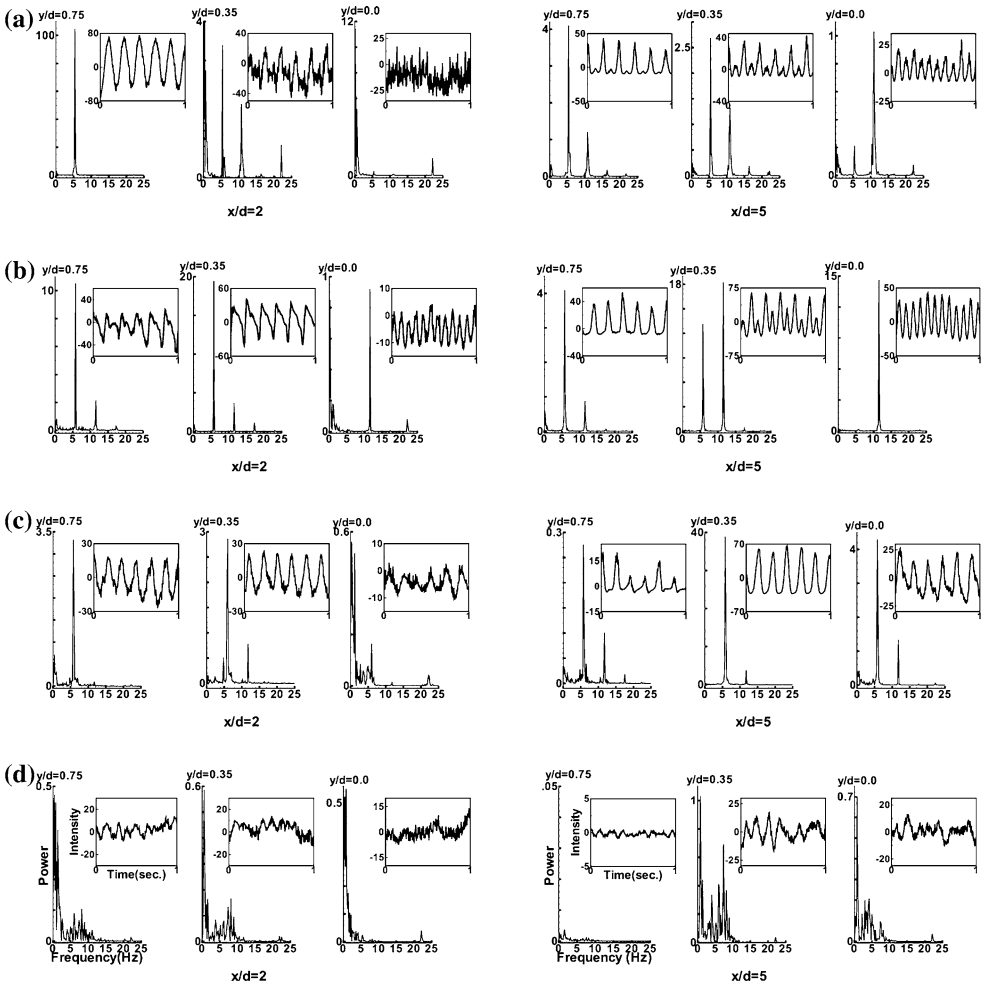

Fig. 10 Power spectra and time traces of light intensity at various stream wise and transverse locations for a square cylinder at Re = 109. **a** Ri = 0.059, **b** Ri = 0.108, **c** Ri = 0.124, and **d** Ri = 0.155. Time traces are shown for 1 s

harmonics in the inner region, in contrast to that at smaller Richardson number. The velocity-time intensity variation also confirms regular periodicity in intensity variation at all stream-wise and transverse locations for Ri = 0.124. No higher harmonics are present near the centerline, y/d = 0. This can be attributed to the modification of shedding from symmetric to straight slender structures, Fig. 5d.

The power spectra at Ri = 0.155 show absence of any clear peak and there is a broadband spectra (Fig. 10d). Regular vortex shedding is now suppressed at this Richardson number. The time traces show irregular small scale random variation. The spectra evolving from being highly peaked at the vortex shedding frequency to a broadband appearance show the disappearance of vortex shedding. The visualization images in Fig. 5d shows the detached vortical structures to be of unsymmetrical slender shape. The flow visualization images in Fig. 5e show mild unsteadiness of the shear layer without any regular shedding. Hence, the increase in the Richardson number leads to inhibition of shedding process and oscillation of the shear layer. The spectra and time traces at a downstream location (x/d = 5.0) show that vortex shedding strength grow differently in the transverse direction compared to the earlier x/d = 2 location. The harmonic spectral peak amplitude is stronger at x/d = 5 compared to that at x/d = 2 for Ri = 0.059. This is due to the greater interaction between the opposite shear layer at downstream location. Overall, the spectra and time traces at the downstream location show similar path to vortex shedding suppression as a function of Richardson number.

The overall behavior of power spectra for the square cylinder is similar to that of the circular cylinder indicating identical influence of buoyancy. A comparison of the time traces of the circular cylinder with the square shows that the shedding characteristics of the two are similar. Frequency doubled harmonics are seen in each set of experiments close to the midplane above the cylinder.

4.7 Velocity profiles

The x-component velocity profiles across the wake of the heated square cylinder as a function of Richardson number are presented in Fig. 11. Data has been presented at a stream wise location of x/d = 13. Measurements have been

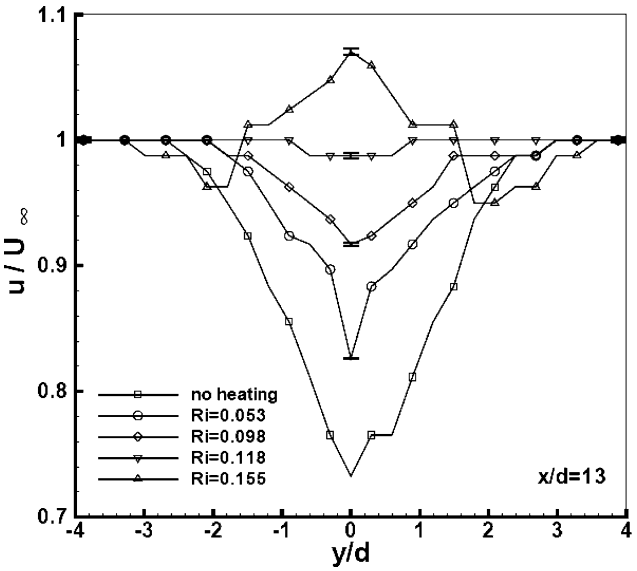

Fig. 11 Stream wise velocity profile across the wake of a heated square cylinder as a function of Richardson number. The stream wise location selected for the plot is x/d = 13. Re = 110

carried out using a pitot static tube with a high-resolution differential pressure digital micro-manometer. The Reynolds number based on the undisturbed flow condition is 110. The velocity measurements are influenced by changes in temperature of the fluid. To quantify the maximum error in the velocity measurement (at x/d = 13) on account of high-fluid temperature in the wake, temperature measurement has been carried out by placing a thermocouple at the wake center-plane. A maximum increase of 1.5–2.0°C in the centerline temperature was observed at the highest heating level. The related maximum uncertainty in velocity measurement is shown as an error bar in the centerline data in Fig. 11. The maximum uncertainty in velocity measurement is found to be <0.3%.

Velocity profile at cylinder surface temperatures of 45, 60, 67, and 80°C are compared in Fig. 11 with the unheated cylinder. The maximum heating level at a Richardson number of 0.155 in Fig. 11 corresponds to suppressed vortex shedding. The velocity deficit of the wake is seen to decrease with an increase in Richardson number. The wake size, i.e., the transverse extent of the low-velocity region reduces with an increase in Richardson number. At a Richardson number of 0.118, the velocity deficit disappears and the velocity profile is close to uniform. At this point, the buoyancy forces add enough momentum to cancel the momentum deficit due to cylinder. With subsequent increase in Richardson number, the velocity inside the wake increases with respect to the free stream velocity.

Michaux-Leblond and Belorgey (1997) observed increase in velocity magnitude and decrease in wake width behind a circular cylinder in a water tunnel with increase in cylinder temperature. They reported complete suppression of recirculation bubble at higher heat inputs. With an increase in heat input, the increase in the wake velocity can be attributed to the additive effect of buoyancy in an aided flow configuration. The heated cylinder acts as an effective pump or a self-propelled body. Hence, the suppression of vortex shedding can be related to the cancellation effect of thermal pumping and fluid inertia, leading to the disappearance of the velocity deficit. The curvature of the velocity profile in the wake changes due to heating of the cylinder. This modifies the wake instability characteristics. It provides an alternative explanation to elimination of vortex shedding at high Richardson number. The above trends were seen for a circular cylinder as well.

4.8 Temperature distribution

Temperature variation in the wake of a heated square cylinder has been obtained by analyzing schlieren-interferograms. The center of the dark fringe was assumed to be the location of the isotherm. The time-averaged temperature distribution in the wake of a heated square cylinder is shown in form of dimensionless profile in the stream wise direction. The Reynolds number for the present experiment is 109. Temperature profiles are presented in Fig. 12a, b as a function of Richardson number at cylinder centerline (y/d = 0.0) and an offset location (y/d = 0.35), respectively. It is seen that temperature decreases continuously in stream wise direction for both y-locations and for all Richardson numbers. The increase in Richardson number reduces slope of the dimensionless temperature profile. Hence the heated zone spreads over a longer distance downstream. For the centerline data (y/d = 0), the temperature profiles of various Richardson numbers merge over a distance of x/d = 0–0.4. This indicates that heat transfer in the near field region of the cylinder is primarily by diffusion. When y/d = 0.35, the overlap occurs only up to x/d = 0.2. This can be attributed to greater influence of the external flow field in the shear layer than at the centerline. In terms of thermal energy content, the area under the θ-x curve shows that forced convection flow carries the greatest while buoyant convection has the least.

4.9 Convection velocity and phase shift

The convection velocity refers to the average speed of vortex structures. It is useful for observing the flow field in a frame of reference, which translates at the convection velocity. Its value is governed by entrainment, shear layer growth rates and mixing characteristics of the wake.

The convection velocity, u_c, defined as the average traveling velocity of vortex structures is obtained as

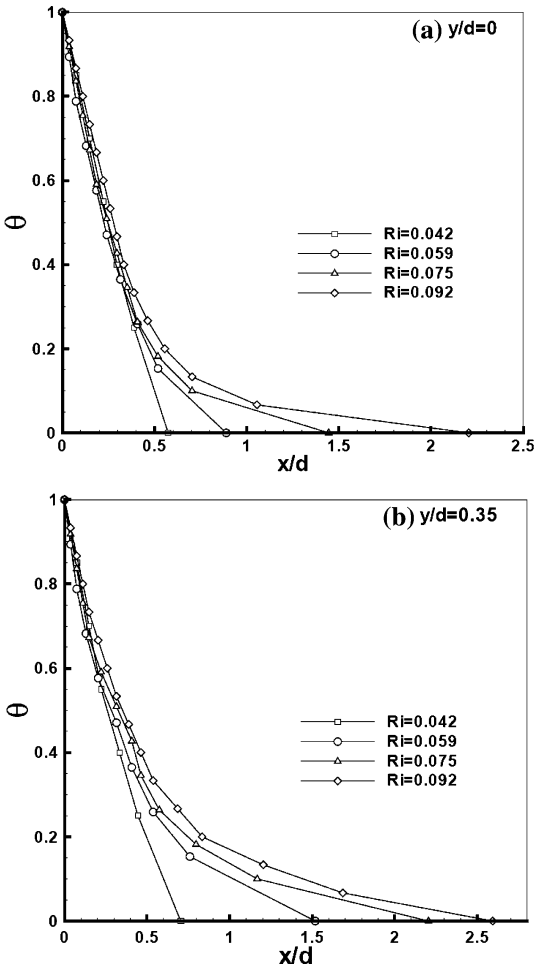

Fig. 12 Dimensionless temperature profiles in the wake of a heated square cylinder as a function of Richardson number. *Re* = 109. **a** *y/d* = 0 and **b** *y/d* = 0.35

follows. A two-dimensional cross-correlation technique is used to track individual structures as they convect downstream (Ben-yaker and Hanson 2002). The large structure (vortex) is identified within a specified window in the first image and is tracked within the specified window in the time delayed image. The interrogation window is selected such that the vortex is first located at the center of the window. The cross-correlation function is calculated at each pixel location of the second image. The point of highest cross-correlation magnitude corresponds to displacement of the structure (Δx) over the time interval considered (Δt). Once displacement is known, the large-scale convection velocity is determined by the formula

$$u_c = \frac{\Delta x}{\Delta t}.$$

Here Δt is the interframing time between images. Displacement is recorded with an uncertainty of ±1 pixel. In the present work, the large-scale structures convect mainly in the stream wise direction. Details of efficient calculation of cross-correlation including selection of window size and interframing time are discussed by Smith and Dutton (1999) and Ben-yaker and Hanson (2002). Three shedding cycles have been considered for tracking vortical structures to ascertain cycle-to-cycle variations. The convection velocity was found to be equal for each oscillation cycle with an uncertainty of ±4.8%.

Figure 13a, b show the variation of the non-dimensional stream wise convection velocity behind a square cylinder as a function of the dimensionless stream wise coordinate at Reynolds numbers of 109 and 118 and increasing Richardson number. For the range of parameters considered, it is clear that u_c/U_∞ increases from 0.35 to 0.85 over $2.7 \leq x/d \leq 5.2$. This trend does not depend significantly on Reynolds number. The effect of heating increases the length of the base region and the instant of vortex detachment from the cylinder is delayed. Subsequently,

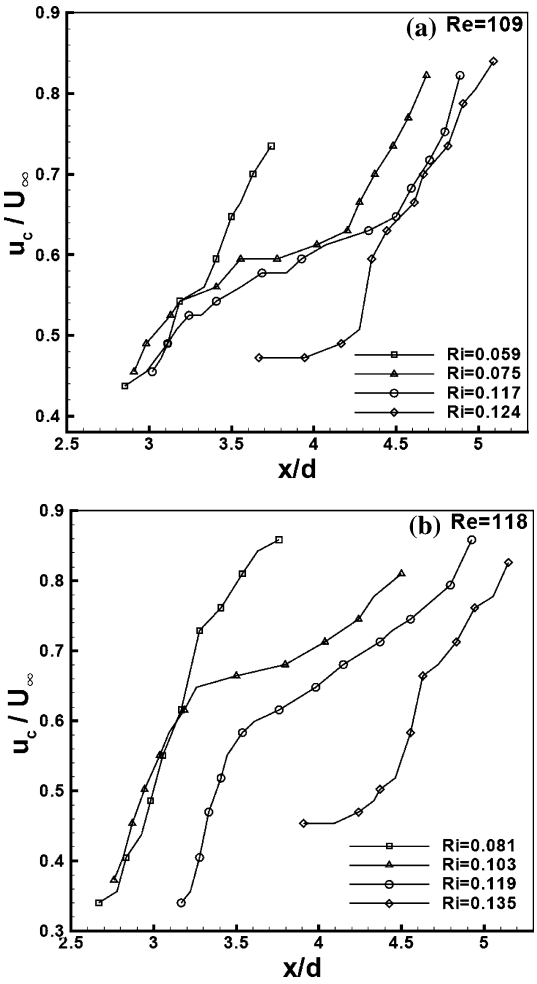

Fig. 13 Non-dimensional convection velocity of vortex structures as a function of the stream wise coordinate in the wake of a heated square cylinder. **a** *Re* = 109; **b** *Re* = 118

when shedding is initiated, structures attain similar asymptotic speeds. The convection velocity at a given location is, however lower for a higher Richardson number. The convection velocity falls to zero beyond the critical Richardson number.

For small Richardson number, i.e., at $Ri = 0.059$, the nature of convection velocity variation in the stream wise direction is similar to that observed in a circular cylinder wake (Lin and Hsieh 2003). Lin and Hsieh (2003) observed the convection velocity to increase from $0.5 \times U_\infty$ to $0.8 \times U_\infty$ at $Re = 160$. In present case (Fig. 13a), the convection velocity increases from $0.44 \times U_\infty$ to $0.74 \times U_\infty$ at $Re = 109$ for square cylinder. The variation of convection velocity in the stream wise direction changes with an increase in Richardson number. In the near field region ($x/d < 4$), the slope of the convection velocity variation is lower when compared to that in the far field at higher Richardson numbers ($Ri = 0.075$, 0.117, and 0.124). This indicates that the wake can be broadly categorized into two zones; the near field zone, in which diffusion due to viscosity and thermal effects influence the vortex motion and the far field zone, in which inertia and buoyancy effects dominate. Therefore, differing slopes in the convection velocity variation are observed at two Reynolds number ($Re = 109$ and 118), Fig. 13. Overall, heating influences the time evolution of vortex structures in the wake of the heated cylinder when compared to that of an unheated cylinder.

The cross-spectrum, defined as the Fourier transform of the cross-correlation function is useful in obtaining the nature of vortex shedding as symmetric or alternate. It provides the degree of correlation between perturbations of equal frequency recorded at two different spatial locations. The phase difference (ϕ) between the two signals at a frequency f is obtained from the real ($Re(f)$) and imaginary parts ($Im(f)$) of the cross-spectrum as:

$$\phi = \tan^{-1}\left[\frac{\mathrm{Im}(f)}{\mathrm{Re}(f)}\right].$$

The evolution of phase shift of vortex structures between two stream wise locations is reported in Fig. 14 as a function of Richardson number. The phase difference between $x/d = 2$–3.5 and $x/d = 2$–5 for $y/d = 0.75$ as a function of Richardson number is reported for $Re = 109$ and 119. The stream wise locations ($x/d = 2$, 3.5, and 5) have been selected to obtain the coherence of vortical structures in the near field and far field region. As expected, the phase difference between $x/d = 2$ and 5 is higher than that between $x/d = 2$ and 3.5 locations. It is seen that an increase in Richardson number increases the phase difference of the vortex structures. Equivalently, it reduces the convection velocity of vortices. The increase in phase

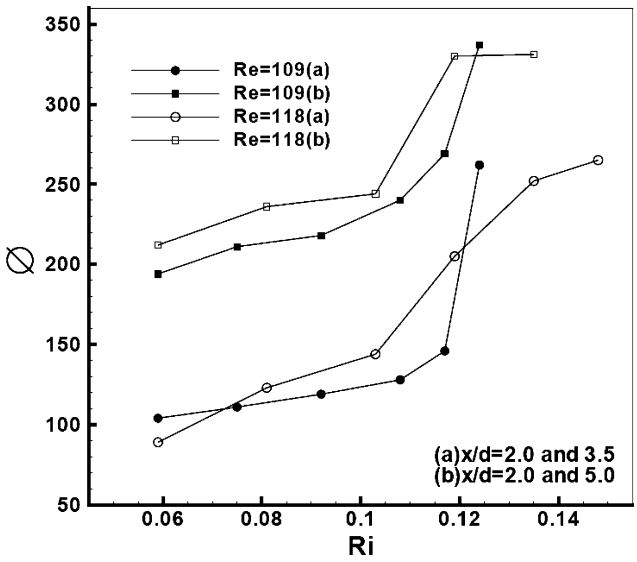

Fig. 14 Variation of phase shift between two stream wise locations in the wake of a heated square cylinder with Richardson number. The transverse location selected is $y/d = 0.75$

difference of vortex structure is gradual at lower Richardson numbers, but shows a sharp increase at higher Richardson numbers. This indicates that in the near field region, the phase evolution is primarily related to the temperature dependent fluid properties. In the far field, the buoyancy induced vortex interaction influences the evolution of vortex structures.

4.10 Instability mechanism

To understand the mechanism of vortex shedding suppression by heat input, the physics of vortex formation needs to be understood. Gerrard (1966) proposed that the vortex street is a function of the formation length, specifically, the relative scales of formation and diffusion regions. According to this model, the circulation in the shear layer must be sufficient to draw the opposite shear layer across the wake center-plane. This interaction must take place before the formation length is reached. The vortex street is suppressed if vorticity in the shear layer diffuses over a critical diffusion length and shear layers are prevented from interactions over a critical formation length. The time-averaged images of the present work (Figs. 6, 7) show that with an increase of heat input, the length of the base region increases and the instant of vortex detachment from the cylinder is delayed, leading to an increase in the formation length. The instantaneous visualization images show the shape of vortex structures become slender-like at a higher Richardson number. The power spectra show absence of multiple peaks in the cylinder centerline at higher Richardson number (Fig. 10). This indicates the reduction

in the circulation of these structures as well as interaction between neighboring vortex structures of the opposite shear layers. Owing to an increase in formation length, these structures rub each other from opposite sides. The transverse interaction between the shear layers is however insignificant. The slender vortices behave as a single plume oscillating at the shedding frequency. The plume becomes steady at the critical value of heat input. The u-velocity profile in the wake shows that buoyancy forces accelerate the fluid in the boundary layer and balance the deceleration of fluid caused by an adverse pressure gradient. Buoyancy adds enough momentum to reduce and finally stop the entrainment of the ambient fluid into the wake.

A schematic describing mechanisms of vortex formation and its evolution behind a heated cylinder is shown in Fig. 15. At a lower heating level, the size of the recirculation bubble and the formation length of vortex shedding increase with increase in Richardson number. This may be attributed to the cancellation of inertial vorticity content by the baroclinic vorticity production of density gradient. However, additional momentum of buoyancy regularizes the vortex shedding initially at lower Richardson numbers. With subsequent increase in Richardson number, the formation length of vortex shedding is higher and there is a transformation to slender vortical structures. At this heating level, there is minimal interaction between vortices of opposite shear layers in the sense that there is no feeding of circulation between these shear layers for the growing vortex bubble before commencement of shedding. With subsequent increase in Richardson number, the recirculation bubble disappears due to sufficient momentum injected by buoyancy. The flow field behind the cylinder appears as a natural convection plume.

5 Conclusions

The present study investigates the effect of buoyancy on wake instability of heated circular and square cylinders. Temporally resolved schlieren imaging has been used as a tool for qualitative flow visualization and quantitative measurements of dynamical behavior of vortical structures. The results presented established that control of vortex shedding behind both circular and square cylinders can be realized by heating the cylinder. The vortex shedding frequency is a function of Reynolds number and Richardson number. With an increase of Richardson number, the shedding frequency increases owing to the aiding buoyancy force. However, vortex shedding abruptly ceases at and beyond a certain critical Richardson number which is a function of Reynolds number. This trend is seen for both the square and the circular cross-sections. The Strouhal number, time traces, power spectra, convection velocity of large structures, velocity profile across the wake, phase evolution, and visualization of vortex structures are reported. The mechanism leading to the suppression of vortex shedding has been proposed from these detailed investigations.

The increase in cylinder surface temperature leads to an increase in the inception length of vortex shedding and the size of the recirculation bubble. The vortex structure is transformed to slender shape before suppression of vortex shedding. The absence of multiple peaks in power spectra at the centerline indicates minimal interaction between the vortices in the opposite shear layers at this Richardson number. The buoyancy induced structures cancel the vorticity content of the growing vortex and the feeding of circulation from the opposite shear layers. At the critical Richardson number, the growing vortex cannot sustain its

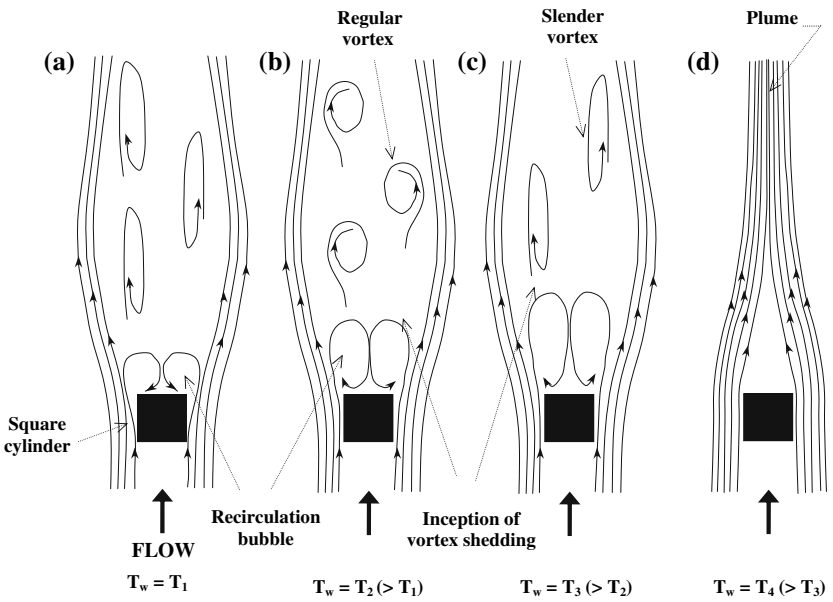

Fig. 15 Schematic sketch of flow patterns that show the progressive suppression of vortex shedding of a heated square cylinder

growth to reach a critical size before shedding is initiated. The mechanism of vortex suppression is primarily related to the influence of heating on the growing vortex inside the shear layer and its circulation content. The convection velocity of vortex structures drops with increase in Richardson number due to the modification of mixing and entrainment. The phase evolution of vortex structures in the downstream direction is also influenced by cylinder heating. Hence, a combined influence on both near field and far field flow structures leads to suppression of vortex shedding behind a heated cylinder. Diffusion due to viscosity and thermal effects is dominant in the near field, while, inertia and buoyancy induced flow structures dominate the far field region. The Reynolds number calculated using kinematic viscosity at the cylinder surface temperature shows a near constant critical value at which vortex shedding is suppressed. This observation is in contrast to the horizontal mean flow experiments, where an effective temperature based on initiation of vortex shedding successfully characterizes wake instability. The similarities in schlieren visualization images, time traces and power spectra between heated circular and square cylinders indicate that the two experience similar mechanisms for vortex shedding suppression.

References

Anderson RC, Milton JE (1989) A large aperture inexpensive interferometer for routine flow measurements. In: IEEE Conference Proceedings on Instrumentation in aerospace simulation facilities, 18–21 September 1989, ICIASF'89 record 10.1109/ICIASF, 1989, 77693, pp 394–399

Badr HM (1984) Laminar combined convection from a horizontal cylinder-parallel and contra flow regimes. Int J Heat Mass Transf 27(1):15–27

Ben-yaker A, Hanson RK (2002) Ultra-fast-framing schlieren system for studies of the time evolution of jets in supersonic cross flows. Exp Fluids 32:652–666

Brackenridge JB, Peterka J (1967) Criteria for quantitative schlieren interferometry. App Opt 6(4):731–735

Chang KS, Sa JY (1990) The effect of buoyancy on the vortex shedding in the near wake of a circular cylinder. J Fluid Mech 220:253–266

Dumouchel F, Lecordier JC, Paranthoen P (1998) The effective Reynolds number of a heated cylinder. Int J Heat Mass Transf 41(12):1787–1794

Gerrard JH (1966) The mechanics of the formation region of vortices behind bluff bodies. J Fluid Mech 25:401–413

Goldstein RJ (ed) (1996) Fluid mechanics measurements, 2nd edn. Taylor and Francis, New York

Jain PC, Lohar BL (1979) Unsteady mixed convection heat transfer from a horizontal circular cylinder. Trans ASME J Heat Transf 101:126–131

Konstantinidis E, Balabani S, Yianneskis M (2003) The effect of flow perturbations on the near wake characteristics of a circular cylinder. J Fluids Struct 18:367–386

Lecordier JC, Browne LWB, Masson SL, Dumouchel F, Paranthoen P (2000) Control of vortex shedding by thermal effect at low Reynolds numbers. Exp Th Fluid Sc 21:227–237

Lin C, Hsieh SC (2003) Convection velocity of vortex structures in the near wake of a circular cylinder. ASCE J Eng mech 129(10):1108–1118

Luo SC, Chew YT, Ng YT (2003) Characteristics of square cylinder wake transition flow. Phys Fluids 15(9):2549–2559

Maas WJPM, Rindt CCM, van Steenhoven AA (2003) The influence of heat on the 3D-transition of the von Karman vortex street. Int J Heat Mass Transf 46:3069–3081

Merkin JH (1977) Mixed convection from a horizontal circular cylinder. Int J Heat Mass Transf 20:73–77

Michaux-Leblond N, Belorgey M (1997) Near wake behavior of a heated circular cylinder: viscosity-buoyancy duality. Exp Therm Fluid Sci 15:91–100

Muralidhar K (2001) Temperature field measurement in buoyancy-driven flows using interferometric tomography. Annu Rev Heat Transf 12:265–376

Noto K, Ishida H, Matsumoto R (1985) A breakdown of the Karman vortex street due to natural convection. Flow visualization III. Springer, Berlin, pp 348–352

Oosthuizen PH, Madan S (1971) The effect of flow direction on combined convective heat transfer from cylinders to air. Trans ASME C J Heat Transf 93:240–242

Robichaux J, Balachandar S, Vanka SP (1999) Three-dimensional Floquet instability of the wake of a square cylinder. Phys Fluids 11(3):560–578

Schumm M, Berger E, Monkewitz PA (1994) Self-excited oscillations in the wake of two-dimensional bluff bodies and their control. J Fluid Mech 271:17–53

Settles GS (2001) Schlieren and shadowgraph techniques: visualizing phenomenon in transparent media. Springer, New York

Sharma A, Eswaran V (2004) Effect of aiding and opposing buoyancy on the heat and fluid flow across a square cylinder at $Re = 100$. Num Heat Transf A 45:601–624

Shi JM, Gerlach D, Breuer M, Biswas G, Durst F (2004) Heating effect on steady and unsteady horizontal laminar flow of air past a circular cylinder. Phys Fluids 16(12):4331–4345

Smith KM, Dutton JC (1999) A procedure for turbulent structure convection velocity measurements using time-correlated images. Exp Fluids 27:244–250

Sohankar A, Norberg C, Davidson L (1999) Simulation of three-dimensional flow around a square cylinder at moderate Reynolds numbers. Phys Fluids 11(2):288–306

Vit T, Ren M, Travnicek Z, Marsik F, Rindt CCM (2006) The influence of temperature gradient on the Strouhal-Reynolds number relationship for water and air. Exp Therm Fluid Sci. doi:10.1016/j.expthermflusci.2006.08.002

Wang A, Travnicek Z, Chia KC (2000) On the relationship of effective Reynolds number and Strouhal number for the laminar vortex shedding of a heated circular cylinder. Phys Fluids 12(6):1401–1410

Yu MH, Monkewitz PA (1990) The effect of nonuniform density on the absolute instability of two-dimensional inertial jets and wakes. Phys Fluids A 2(7):1175–1181